Probing the Masses and Radii of Donor Stars in Eclipsing X-ray Binaries with the Swift Burst Alert Telescope

Joel B. Coley[1,2], Robin H. D. Corbet[1,2], Hans A. Krimm[3,4]
jcoley1@umbc.edu

ABSTRACT

Physical parameters of both the mass donor and compact object can be constrained in X-ray binaries with well-defined eclipses, as our survey of wind-fed supergiant X-ray binaries (SGXBs) IGR J16393-4643, IGR J16418-4532, IGR J16479-4514, IGR J18027-2016 and XTE J1855-026 reveals. Using the orbital period and Kepler's third law, we express the eclipse half-angle in terms of radius, inclination angle and the sum of the masses. Pulse-timing and radial velocity curves can give masses of both the donor and compact object as in the case of the "double-lined" binaries IGR J18027-2016 and XTE J1855-026. The eclipse half angles are 15^{+3}_{-2}, $31.7^{+0.7}_{-0.8}$, 32±2, 34±2 and 33.6±0.7 degrees for IGR J16393-4643, IGR J16418-4532, IGR J16479-4514, IGR J18027-2016 and XTE 1855-026, respectively. In wind-fed systems, the primary not exceeding the Roche-lobe size provides an upper limit on system parameters. In IGR J16393-4643, spectral types of B0 V or B0-5 III are found to be consistent with the eclipse duration and Roche-lobe, but the previously proposed donor stars in IGR J16418-4532 and IGR J16479-4514 were found to be inconsistent with the Roche-lobe size. Stars with spectral types O7.5 I and earlier are possible. For IGR J18027-2016, the mass and radius of the donor star lie between 18.6–19.4 $M_\odot$ and 17.4–19.5 $R_\odot$. We constrain the neutron star mass between 1.37–1.43 $M_\odot$. We find the mass and radius of the donor star in XTE J1855-026 to lie between 19.6–20.2 $M_\odot$ and 21.5–23.0 $R_\odot$. The neutron star mass was constrained to 1.77–1.82 $M_\odot$. Eclipse profiles are asymmetric in IGR J18027-2016 and XTE J1855-026, which we attribute to accretion wakes.

1. Introduction

High-Mass X-ray Binaries (HMXBs) are relatively young systems, which consist of a compact object (neutron star or black hole) and an early-type OB star orbiting the common center of mass. First discovered in the 1970s, HMXBs are split into two individual classes–Be X-ray binaries (BeXBs) and supergiant X-ray binaries (SGXBs). BeXBs are transient systems where the compact object is in a wide, typically eccentric, orbit (P$\gtrsim$10 days) around a rapidly rotating non-supergiant B-type star. The primary mode of mass transfer occurs when the compact object passes through the circumstellar decretion disc of the mass donor. In SGXBs, the compact object is in a short (∼1–42 day) orbit around an OB-supergiant where the accretion mechanism is either via the powerful stellar wind and/or Roche-lobe overflow. While the eccentricity in most SGXBs with short orbital periods is near zero, some SGXBs host compact objects in highly eccentric orbits (e.g. GX 301-2 Islam & Paul 2014). In wind-accretors, the X-ray luminosity is on the order of 10^{35}–10^{36} erg s^{-1}. However, a much higher luminosity is found in systems where the donor fills its Roche-lobe, $\sim10^{38}$ erg s^{-1} (Kaper et al. 2004).

Many HMXBs host a neutron star where modulation is often seen at its rotation period. The

[1]University of Maryland,Baltimore County, MD, USA
[2]CRESST/Mail Code 662, X-ray Astrophysics Laboratory, NASA Goddard Space Flight Center, Greenbelt, MD 20771, USA
[3]Universities Space Research Association, 7178 Columbia Gateway Drive, Columbia, MD 21046, USA
[4]CRESST/Mail Code 661, X-ray Astroparticle Physics Laboratory, NASA Goddard Space Flight Center, Greenbelt, MD 20771, USA

mass of the neutron star can be constrained in eclipsing X-ray pulsars, which can lead to an improved understanding of the neutron star Equation of State (Mason et al. 2011, and references therein). Currently, the neutron star mass has been constrained in 10 XRBs where the lower limit for each object corresponds to edge-on orbital inclinations and the upper limit is calculated when the donor star just fills its Roche-lobe. While over 100 Equations of State have been proposed (Kaper et al. 2006), only one model is physically correct (Mason et al. 2010, 2011).

The mass ratio between the neutron star and donor star is equal to the ratio between the semi-amplitude of the radial velocities of the donor star, $K_{\rm O}$, and the neutron star, $K_{\rm X}$. Throughout the paper, we use a definition of mass ratio, q, as the ratio of the compact object mass to that of the donor star mass (Joss & Rappaport 1984). The orbital period of the binary, P, and $K_{\rm X}$ can be calculated using pulse-timing analysis (Val Baker et al. 2005, and references therein), which is analogous to measuring the Doppler shift of spectral lines in the optical and/or near-infrared (Joss & Rappaport 1984). The projected semi-major axis can be determined from the semi-amplitude of the radial velocity of the neutron star. The semi-amplitude of the radial velocity of the donor star can be determined using optical and/or near-infrared spectroscopic information.

Eclipse measurements can also be exploited as timing markers to determine the binary orbital evolution of HMXBs. A significant orbital period derivative, $\dot{P}$, was previously found in several eclipsing HMXBs (e.g 4U 1700-377; SMC X-1; Cen X-3; LMC X-4 and OAO 1657-415, Rubin et al. 1996; Raichur & Paul 2010; Falanga et al. 2015) and can be used to investigate the orbital evolution over long periods of time. While several contending theories to explain the orbital decay have been investigated, the most probable explanations involve tidal interaction and rapid mass transfer between the components of the binary systems (Falanga et al. 2015, and references therein).

The *Swift* Burst Alert Telescope (BAT), sensitive to X-rays in the 15–150 keV band (Barthelmy et al. 2005), provides an excellent way to study highly absorbed SGXBs. The large absorption found in these systems is problematic for instruments such as the *Rossi X-ray Timing Explorer (RXTE)* All Sky Monitor (ASM), which operated in the 1.5–12 keV band (Levine et al. 2011). The sensitivity to higher energy X-rays allows *Swift*-BAT to peer through this absorption (Corbet & Krimm 2013, and references therein).

We present here constraints on the mass and radius of the donor star in eclipsing XRBs. The probability of an eclipse in a supergiant XRB with an orbital period less than 20 d can be expressed in terms of the orbital period, mass of the donor star, and radius of the donor star (Equation 1; Ray & Chakrabarty 2002). The probability of an eclipse in long-period XRBs is low. Using a literature search, we determined HXMB systems where BAT observations can significantly improve the the properties of the stellar components and orbital evolution of the systems using eclipsing properties. Five eclipsing XRBs were identified: IGR J16393-4643, IGR J16418-4532, IGR J16479-4514, IGR J18027-2016 and XTE J1855-026, which are all highly obscured SGXBs. We note while the masses of both the donor and compact object had previously been constrained in IGR J18027-2016, the error on the eclipse half-angle was large at 4.5° (Hill et al. 2005). The error estimates concerning the radius and mass of the donor star are significantly improved in our analysis.

This paper is structured in the following order: *Swift* BAT observations and the description of the eclipse model are presented in Section 2; Section 3 focuses on individual sources that are known to be eclipsing. Section 4 presents a discussion of the results and the conclusions are outlined in Section 5. If not stated otherwise, the uncertainties and limits presented in the paper are at the 1σ confidence level.

2. Data Analysis and Modelling

2.1. Swift BAT

The BAT on board the *Swift* spacecraft is a hard X-ray telescope operating in the 15–150 keV energy band (Barthelmy et al. 2005). The detector is composed of CdZnTe where the detecting area and field of view (FOV) are 5240 $\rm cm^2$ and 1.4 sr (half-coded), respectively (Barthelmy et al. 2005). The BAT provides an all-sky hard X-ray survey with a sensitivity of $\sim$1 mCrab (Tueller et al. 2010). The Crab produces $\sim$0.045 counts $\rm cm^{-2}$ $\rm s^{-1}$ over the entire en-

ergy band.

We analyzed BAT data obtained during the time period MJD 53416–56745 (2005 February 15–2014 March 29). Light curves were retrieved using the extraction of the BAT transient monitor data available on the NASA GSFC HEASARC website[1] (Krimm et al. 2013), which includes orbital and daily-averaged light curves. We used the orbital light curves in the 15–50 keV energy band in our analysis, which have typical exposures of ∼6 min (see Section 3). The short exposures, which are somewhat less than typical *Swift* pointing times (∼20 min), can arise due to the observing plan of *Swift* itself where BAT is primarily tasked to observe gamma-ray bursts (Krimm et al. 2013).

The light curves were further screened to exclude bad quality points. We only considered data where the data quality flag ("DATA_FLAG") was set to 0. Data flagged as "good" are sometimes suspect, where a small number of data points with very low fluxes and implausibly small uncertainties were found (Corbet & Krimm 2013). These points were removed from the light curves. We corrected the photon arrival times to the solar system barycenter. We used the scripts made available on the Ohio State Astronomy webpage[2] In this paper, the barycenter-corrected times are referred to as Barycenter Modified Julian Date (BMJD).

We initially derived the orbital period for each XRB in our sample using Discrete Fourier transforms (DFTs) of the light curves to search for periodicities in the data. We weighted the contribution of each data point to the power spectrum by its uncertainty, using the "semi-weighting" technique (Corbet et al. 2007; Corbet & Krimm 2013), where the error bars on each data point and the excess variability of the light curve are taken into account. We derived uncertainties on the orbital periods using the expression given in Horne & Baliunas (1986).

2.2. Eclipse Modeling

We initially modeled the eclipses using a symmetric "step and ramp" function (see Table 1) where the intensities are assumed to remain constant before ingress, during eclipse and after egress and follow a linear trend during the ingress and egress transitions (Coley et al. 2014). The count rates before ingress, during eclipse and after egress were each considered to be free parameters and were fit as follows: $C_{\rm ing}$ was fit from binary phase ϕ =-0.2 to the start of ingress, $C_{\rm ecl}$ was fit during eclipse and $C_{\rm eg}$ was fit from the end of egress to phase ϕ =0.2 (see Equation 1). While we find the eclipse profiles of IGR J16393-4643, IGR J16418-4532 and IGR J16479-4514 to be symmetric within errors, the profiles show some asymmetry in the cases of IGR J18027-2016 and XTE J1855-026. We note that a symmetric "step and ramp" function could lead to systematic errors and we therefore fit the eclipse profiles using an asymmetric "step and ramp" function (see Equantion 1 and Table 2). The parameters in this model are as follows: the phases corresponding to the start of ingress and start of egress, $\phi_{\rm ing}$ and $\phi_{\rm eg}$, the duration of ingress, $\Delta\phi_{\rm ing}$, the duration of egress, $\Delta\phi_{\rm eg}$, the pre-ingress count rate, $C_{\rm ing}$, the post-egress count rate, $C_{\rm eg}$, and the count rate during eclipse, $C_{\rm ecl}$. The eclipse duration and mid-eclipse phase are calculated using Equations 2 and 3, respectively.

$$C = \begin{cases} C_{\rm ing}, & -0.2 \le \phi \le \phi_{\rm ing} \\ (\frac{C_{\rm ecl}-C_{\rm ing}}{\Delta\phi_{\rm ing}})(\phi-\phi_{\rm ing})+C_{\rm ing}, & \phi_{\rm ing} \le \phi \le \phi_{\rm ing}+\Delta\phi_{\rm ing} \\ C_{\rm ecl}, & \phi_{\rm ing}+\Delta\phi_{\rm ing} \le \phi \le \phi_{\rm egr} \\ (\frac{C_{\rm egr}-C_{\rm ecl}}{\Delta\phi_{\rm eg}})(\phi-\phi_{\rm egr})+C_{\rm ecl}, & \phi_{\rm egr} \le \phi \le \phi_{\rm egr}+\Delta\phi_{\rm eg} \\ C_{\rm eg}, & \phi_{\rm egr}+\Delta\phi_{\rm eg} \le \phi \le 0.2 \end{cases} \quad (1)$$

$$\Delta\phi_{\rm ecl} = \phi_{\rm egr} - (\phi_{\rm ing} + \Delta\phi_{\rm ing}) \quad (2)$$

$$\phi_{\rm mid} = \frac{1}{2}(\phi_{\rm egr} + (\phi_{\rm ing} + \Delta\phi_{\rm ing})) \quad (3)$$

The eclipse duration, time of mid-eclipse, and eclipse half-angle ($\Theta_{\rm e} = \Delta\phi_{\rm ecl}\times 180°$) from fitting the BAT folded light curves for each source are reported in Tables 1– 3. For each source, we initially used an ephemeris based on our determination of the orbital period from the DFT and time of mid-eclipse. Using an 'observed minus calculated' $O-C$ analysis (see Figures 1–3), we refined the orbital periods and improved on the time of mid-eclipse for each XRB in our sample. We note that no eclipses are visible in the unfolded light curves and it is necessary to observe

[1] http://heasarc.gsfc.nasa.gov/docs/swift/results/transients/

[2] http://astroutils.astronomy.ohio-state.edu/time/.

TABLE 1
ECLIPSE MODEL PARAMETERS, ASSUMING A SYMMETRIC ECLIPSE PROFILE

Model Parameter	IGR J16393-4643	IGR J16418-4532	IGR J16479-4514	IGR J18027-2016	XTE J1855-026
$\phi_{\rm ing}$	$-0.079^{+0.006}_{-0.014}$	-0.107±0.002	$-0.114^{+0.003}_{-0.004}$	$-0.150^{+0.005}_{-0.003}$	$-0.131^{+0.001}_{-0.002}$
$\Delta\phi$	$0.040^{+0.009}_{-0.008}$	$0.019^{+0.002}_{-0.003}$	$0.029^{+0.003}_{-0.004}$	$0.053^{+0.004}_{-0.003}$	0.038±0.002
C^a	1.27±0.04	1.18±0.05	1.05±0.06	1.59±0.06	2.64±0.06
$\phi_{\rm egr}$	$0.048^{+0.004}_{-0.005}$	$0.088^{+0.002}_{-0.001}$	$0.092^{+0.003}_{-0.004}$	$0.098^{+0.002}_{-0.004}$	0.094±0.002
$C_{\rm ecl}{}^a$	0.71±0.06	0.00±0.05	0.03±0.05	0.17±0.04	-0.04±0.05
$\Delta\phi_{\rm ecl}$	$0.09^{+0.01}_{-0.02}$	0.175±0.003	$0.177^{+0.005}_{-0.007}$	$0.196^{+0.007}_{-0.005}$	0.187±0.003
$P^b_{\rm orb}$	4.23794±0.00007	3.73880±0.00002	3.31965±0.00006	4.56999±0.00005	6.07410±0.00004
$\dot{P}^c_{\rm orb}$	-5±4	0.7±1.0	3±2	-2±2	0.5±1.0
$T^d_{\rm mid}$	$55074.99^{+0.02}_{-0.04}$	55087.714±0.006	$55081.571^{+0.009}_{-0.012}$	$55083.79^{+0.02}_{-0.01}$	$55079.055^{+0.010}_{-0.009}$
$\Theta^e_{\rm e}$	16^{+2}_{-3}	31.5±0.6	$31.9^{+0.9}_{-1.3}$	35±1	$33.6^{+0.6}_{-0.5}$
χ^2_ν (dof)	1.13(77)	0.84(77)	1.03(77)	0.93(77)	1.23(77)

NOTE.—
[a] Units are 10^{-3} counts cm^{-2} s^{-1}.
[b] Refined orbital periods using an $O-C$ analysis. Units are days.
[c] The orbital period derivative at the 90% confidence interval found using an $O-C$ analysis. Units are 10^{-7} d d^{-1}.
[d] Units are barycentered Modified Julian Time (BMJD). Phase 0 is defined as eclipse center.
[e] Units are degrees.

TABLE 2
ECLIPSE MODEL PARAMETERS, ASSUMING AN ASYMMETRIC ECLIPSE PROFILE

Model Parameter	IGR J16393-4643	IGR J16418-4532	IGR J16479-4514	IGR J18027-2016	XTE J1855-026
$\phi_{\rm ing}$	$-0.092^{+0.008}_{-0.005}$	-0.108±0.002	-0.118±0.003	-0.160±0.005	-0.136±0.002
$\Delta\phi_{\rm ing}$	0.06±0.01	0.020±0.003	0.024±0.008	0.08±0.01	0.042±0.003
$\Delta\phi_{\rm eg}$	0.039±0.006	$0.014^{+0.003}_{-0.004}$	$0.026^{+0.007}_{-0.003}$	$0.018^{+0.005}_{-0.004}$	0.038±0.003
$C_{\rm ing}{}^a$	1.28±0.06	$1.07^{+0.07}_{-0.06}$	1.01±0.08	1.43±0.08	2.44±0.08
$C_{\rm eg}{}^a$	1.26±0.06	1.22±0.07	1.04±0.08	1.67±0.08	$2.79^{+0.09}_{-0.08}$
$\phi_{\rm egr}$	$0.049^{+0.004}_{-0.006}$	0.089±0.002	0.086±0.003	0.112±0.002	$0.092^{+0.001}_{-0.002}$
$C_{\rm ecl}{}^a$	0.69±0.06	0.00±0.05	0.05±0.05	0.14±0.05	-0.05±0.05
$\Delta\phi_{\rm ecl}$	$0.09^{+0.02}_{-0.01}$	0.176±0.004	0.180±0.009	0.19±0.01	0.186±0.004
$P^b_{\rm orb}$	4.23810±0.00007	3.73881±0.00002	3.31961±0.00004	4.56988±0.00006	6.07413±0.00004
$\dot{P}^c_{\rm orb}$	-6±4	0.2±0.8	3±2	-3±4	0.5±1.9
$T^d_{\rm mid}$	55074.99±0.03	$55087.721^{+0.007}_{-0.008}$	55081.57±0.02	55083.88±0.03	55079.07±0.01
$\Theta^e_{\rm e}$	15^{+3}_{-2}	$31.7^{+0.7}_{-0.8}$	32±2	34^{+3}_{-2}	33.6±0.7
χ^2_ν (dof)	1.18(80)	0.97(80)	1.08(80)	1.01(80)	1.03(80)

NOTE.—
[a] Units are 10^{-3} counts cm^{-2} s^{-1}.
[b] Refined orbital periods using an $O-C$ analysis. Units are days.
[c] The orbital period derivative at the 90% confidence interval found using an $O-C$ analysis. Units are 10^{-7} d d^{-1}.
[d] Units are BMJD. Phase 0 is defined as eclipse center.
[e] Units are degrees.

TABLE 3
ECLIPSE MODEL PARAMETERS, INCLUDING HISTORICAL MID-ECLIPSE TIMES

Model Parameter	IGR J18027-2016[a,c]	IGR J18027-2016[a,d]	XTE J1855-026[b,c]	XTE J1855-026[b,d]
$\phi_{\rm ing}$	$-0.147^{+0.004}_{-0.005}$	$-0.167^{+0.005}_{-0.004}$	$-0.131^{+0.001}_{-0.002}$	-0.136±0.002
$\Delta\phi_{\rm ing}$	$0.053^{+0.005}_{-0.007}$	0.082±0.009	0.038±0.002	0.040±0.003
$\Delta\phi_{\rm eg}$	$0.053^{+0.005}_{-0.007}$	$0.027^{+0.004}_{-0.006}$	0.038±0.002	0.037±0.003
$C_{\rm ing}$[e]	1.59±0.05	1.25±0.08	2.64±0.06	2.45±0.08
$C_{\rm eg}$[e]	1.59±0.05	1.68±0.08	2.64±0.06	$2.79^{+0.09}_{-0.08}$
$\phi_{\rm egr}$	0.099±0.003	0.102±0.002	0.094±0.002	$0.092^{+0.001}_{-0.002}$
$C_{\rm ecl}$[e]	0.17±0.04	0.14±0.04	-0.04±0.05	-0.03±0.05
$\Delta\phi_{\rm ecl}$	$0.193^{+0.007}_{-0.009}$	0.19±0.01	0.187±0.003	0.187±0.004
$P^{f}_{\rm orb}$	4.56982±0.00003	4.56993±0.00003	6.07412±0.00003	6.07414±0.00003
$\dot{P}^{g}_{\rm orb}$	0.8±0.9	0.2±1.1	-0.1±0.5	0.0±0.5
$T^{h}_{\rm mid}$	55083.78±0.01	55083.82±0.01	55079.056±0.009	55079.07±0.01
$\Theta^{i}_{\rm e}$	35±1	34±2	$33.6^{+0.5}_{-0.6}$	33.7±0.7
χ^2_ν (dof)	1.20(77)	0.93(80)	1.02(77)	1.05(80)

NOTE.—
[a] Includes the mid-eclipse times derived in Hill et al. (2005), Jain et al. (2009) and Falanga et al. (2015).
[b] Includes the mid-eclipse times derived in Corbet & Mukai (2002) and Falanga et al. (2015).
[c] Assuming a Symmetric Eclipse Profile.
[d] Assuming an Asymmetric Eclipse Profile.
[e] Units are 10^{-3} counts cm^{-2} s^{-1}.
[f] Refined orbital periods using an $O-C$ analysis. Units are days.
[g] The orbital period derivative at the 90% confidence interval found using an $O-C$ analysis. Units are 10^{-7} d d^{-1}.
[h] Units are BMJD. Phase 0 is defined as eclipse center.
[i] Units are degrees.

multiple cycles of folded light curves in order for eclipses to be seen. We divide the light curves into five equal time intervals (∼670 days), with the exception of IGR J16393-4643 (see Section 3.1), and calculate the mid-eclipse epoch for each interval (see Table 4) In the cases of IGR J18027-2016 and XTE J1855-026, we combine our derived mid-eclipse times with those reported in the literature (Falanga et al. 2015, and references therein). We note that while mid-eclipse times were previously derived for both IGR J16393-4643 and IGR J16479-4514 (see Table 5), these were not used since no error estimate was reported (Islam et al. 2015; Bozzo et al. 2009). We then fit the mid-eclipse times using the orbital change function (see Equation 4) where n is the number of binary orbits given to the nearest integer, $P_{\rm orb}$ is the orbital period in days, $\dot{P}_{\rm orb}$ is the period derivative at T_0, and the error on the linear term is the orbital period error. In all five cases, we improve the error estimate on the orbital period by nearly an order of magnitude (see Section 3). We do not find a significant $\dot{P}_{\rm orb}$ for any source (see Tables 1– 3).

$$T_{\rm n} = T_0 + nP_{\rm orb} + \frac{1}{2}n^2 P_{\rm orb}\dot{P}_{\rm orb} \qquad (4)$$

X-ray binaries that are eclipsing have an eclipse duration that is only dependent on the radius of the mass donor, inclination angle of the system and the orbital separation of the components provided that the orbit is circular ($e = 0$). Using the observed orbital period and Kepler's third law, the duration can be written in terms of the sum of the donor star and compact object masses, which stipulates that the eclipse half-angle, $\Theta_{\rm e}$, can now be expressed in terms of the radius, inclination and masses of the components. In one set of calculations, we assume a $1.4\,M_{\odot}$ compact object which may be appropriate for an accreting neutron star (Chandrasekhar 1931). The region allowed by the measured eclipse half-angle for each binary in Mass-Radius space is shown in Section 3. The inclination is constrained between edge-on orbits (left boundary of the dark shaded region) and close to face-on orbits (the right boundary of the light shaded region). We can attach additional constraints assuming that the mass donor underfills the Roche-lobe (right boundary of the dark shaded region), which is dependent on the mass ratio of the system and the orbital separation. To calculate the eclipse half-angle and the Roche-lobe radius, we used Equation 7 in Joss & Rappaport (1984), also used by Rubin et al. (1996), and Equation 2 in Eggleton (1983), respectively. Further constraints on the parameters of the donor star are imposed with pulse-timing techniques (dashed red lines in Figures 15 and 18). For the systems where pulse-timing results were not available, we additionally calculated the minimum inclination angle of the system, $i_{\rm min}$, that is consistent with the measured eclipse half-angle (see Table 1).

When the semi-amplitude of the radial velocities of both the compact object and the mass

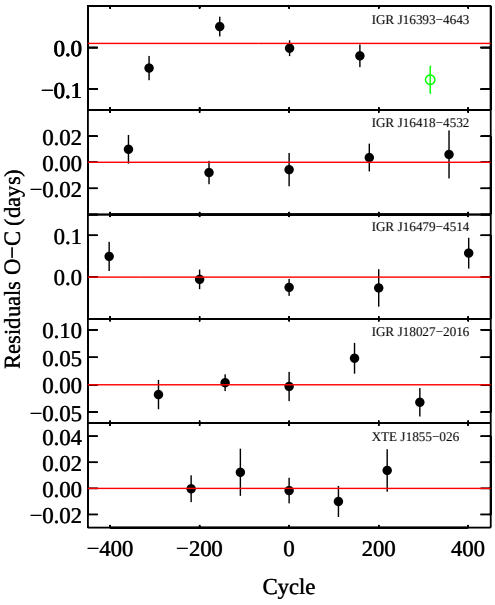

Fig. 1.— The observed minus calculated $(O-C)$ eclipse time residuals for IGR J16393-4643 (top), IGR J16418-4532 (second panel), IGR J16479-4514 (middle), IGR J18027-2016 (fourth panel) and XTE J1855-026 (bottom) fit using a symmetric step-and-ramp function. We subtract the best linear polynomial fit for each source and correct the orbital periods accordingly. For IGR J16393-4643 (top) we only use the first four points to obtain a good fit (see Section 3.1).

TABLE 4
MID-ECLIPSE TIME MEASUREMENTS FOR $O-C$ ANALYSIS

Source	Orbital Cycle (N)	Mid-eclipse time[a] (MJD)	Mid-eclipse time[b] (MJD)
IGR J16393-4643	-313	53748.46±0.03	53748.44±0.03
IGR J16393-4643	-155	$54418.15^{+0.04}_{-0.02}$	$54418.14^{+0.04}_{-0.03}$
IGR J16393-4643	1	$55079.22^{+0.07}_{-0.02}$	$55079.22^{+0.03}_{-0.02}$
IGR J16393-4643	158	$55744.55^{+0.02}_{-0.03}$	$55744.54^{+0.02}_{-0.08}$
IGR J16393-4643	315	... [c]	... [c]
IGR J16418-4532	-359	53745.50±0.01	$53745.491^{+0.013}_{-0.009}$
IGR J16418-4532	-179	$54418.461^{+0.009}_{-0.010}$	54418.468±0.009
IGR J16418-4532	0	55087.71±0.01	55087.72±0.01
IGR J16418-4532	179	$55756.963^{+0.011}_{-0.008}$	55756.967±0.009
IGR J16418-4532	357	56422.47±-0.02	$56422.47^{+0.02}_{-0.01}$
IGR J16479-4514	-402	$53747.19^{+0.02}_{-0.03}$	$53747.21^{+0.02}_{-0.03}$
IGR J16479-4514	-200	54417.63±0.02	$54417.61^{+0.03}_{-0.02}$
IGR J16479-4514	0	$55081.47^{+0.03}_{-0.02}$	$55081.48^{+0.02}_{-0.03}$
IGR J16479-4514	200	$55745.33^{+0.03}_{-0.04}$	55745.28±0.04
IGR J16479-4514	401	$56412.60^{+0.06}_{-0.04}$	$56412.59^{+0.03}_{-0.04}$
IGR J18027-2016	-292	$53749.41^{+0.05}_{-0.03}$	$53749.40^{+0.04}_{-0.05}$
IGR J18027-2016	-143	54430.32±0.02	$54430.34^{+0.04}_{-0.02}$
IGR J18027-2016	0	$55083.79^{+0.02}_{-0.03}$	$55083.85^{+0.08}_{-0.03}$
IGR J18027-2016	146	55751.02±0.03	$55751.06^{+0.03}_{-0.04}$
IGR J18027-2016	292	$56418.12^{+0.02}_{-0.03}$	$56418.20^{+0.03}_{-0.04}$
XTE J1855-026	-219	53748.82±0.01	53748.84±0.01
XTE J1855-026	-109	54416.99±0.02	54416.99±0.02
XTE J1855-026	0	55079.05±0.01	$55079.09^{+0.02}_{-0.03}$
XTE J1855-026	110	55747.20±0.01	55747.21±0.02
XTE J1855-026	219	56409.30±0.02	56409.33±0.02

NOTE.—[a] Obtained using the symmetric step-and-ramp function.
[b] Obtained using the asymmetric step-and-ramp function.
[c] A bad fit for IGR J16393-4643 was obtained in the mid-eclipse time between MJD 56079–56745.

TABLE 5
HISTORIC MID-ECLIPSE TIME MEASUREMENTS FOR IGR J18027-2016 AND XTE J1855-026

Source	Orbital Cycle (N)	Mid-eclipse time (MJD)	Satellite (MJD)	Reference
IGR J16393-4643	-391	53417.955	*Swift*	Islam et al. (2015)
IGR J16479-4514	-161	54547.05418	*Swift*	Bozzo et al. (2009)
IGR J18027-2016	-638	52168.22±0.12	*BeppoSAX*	Augello et al. (2003)
IGR J18027-2016	-638	52168.26±0.04	*BeppoSAX*	Hill et al. (2005)
IGR J18027-2016	-471	52931.37±0.04	*INTEGRAL*	Hill et al. (2005)
IGR J18027-2016	-399	53260.37±0.07	*INTEGRAL*	Jain et al. (2009)
IGR J18027-2016	-286	53776.82±0.07	*Swift*	Jain et al. (2009)
IGR J18027-2016	-267	53863.10±0.14	*INTEGRAL*	Falanga et al. (2015)
IGR J18027-2016	-127	54503.38±0.07	*Swift*	Jain et al. (2009)
XTE J1855-026	-590	51495.25±0.02	*RXTE*	Corbet & Mukai (2002)
XTE J1855-026	-391	52704.04±0.05	*INTEGRAL*	Falanga et al. (2015)
XTE J1855-026	-176	54009.97±0.05	*INTEGRAL*	Falanga et al. (2015)
XTE J1855-026	-31	54890.68±0.05	*INTEGRAL*	Falanga et al. (2015)

NOTE.—Historical mid-eclipse times for IGR J16479-4514, IGR J18027-2016 and XTE J1855-026 found using *RXTE*, *Swift* BAT and *INTEGRAL*.

donor are known (e.g. IGR J18027-2016, XTE J1855-026), the mass ratio between the compact object and mass donor can be calculated (Equation 6, Joss & Rappaport 1984). This means that in addition to the radius and mass of the donor star, the mass of the compact object can be constrained. The mass of the donor star can be written in terms of the semi-amplitude of the radial velocity of the compact object, orbital period, Newton's gravitational constant, inclination angle of the system and the mass ratio (Joss & Rappaport 1984). Likewise, the compact object mass can be written in terms of the semi-amplitude of the of the radial velocity of the donor star, orbital period, Newton's gravitational constant, inclination angle of the system and the mass ratio (Joss & Rappaport 1984). To calculate the masses of both the donor star and the compact object, we used Equations 2 and 3 in Ash et al. (1999), also used by Rappaport & Joss (1983).

For consistency, we compare our derived constraints on the masses and radii of the donor stars with those expected for the previously proposed spectral types. For the systems where pulse-timing results were not available, we calculate the predicted eclipse half-angles as a function of inclination angle using the mass and radius for the derived spectral types (see Section 3). Generally we used results from Carroll & Ostlie (2006) for main-sequence, giant and supergiant luminosity classes. These are represented by the red, green and blue dashed lines in mass-radius space for each system (see Section 3). For O-type supergiants, we also use Tables 3 and 6 in Martins et al. (2005) to compare our results (see blue dotted lines in Figures 6, 9 and 12). The constraints for B-type supergiants are additionally compared with Tables 3 and 6 in Lefever et al. (2007) for B-type supergiants (blue crosses in Figures 15 and 18).

3. Five Eclipsing HMXBs

3.1. IGR J16393-4643 (=AX J16390.4-4642)

IGR J16393-4643 is an HMXB first discovered and listed as AX J16390.4-4642 in the *ASCA* Faint Source Catalog (Sugizaki et al. 2001) and was later detected with *INTEGRAL* (Bodaghee et al. 2006). The average flux in the 20–40 keV band was found to be 5.1×10^{-11} erg cm^{-2} s^{-1}, and intensity variations were found to exceed a factor of 20 (Bodaghee et al. 2006). In the 2–10 keV

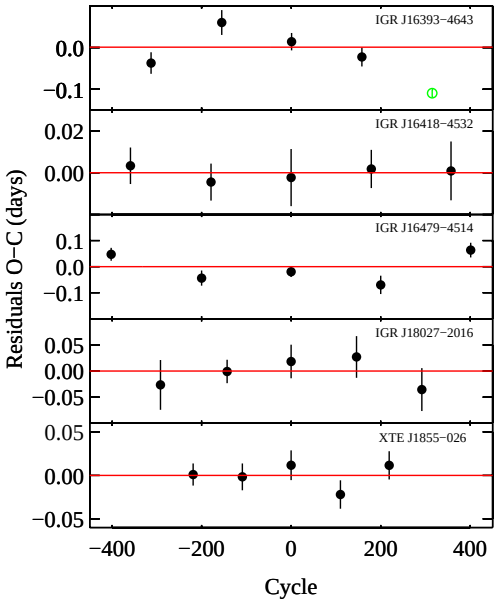

Fig. 2.— The observed minus calculated ($O-C$) eclipse time residuals for IGR J16393-4643 (top), IGR J16418-4532 (second panel), IGR J16479-4514 (middle), IGR J18027-2016 (fourth panel) and XTE J1855-026 (bottom) fit using an asymmetric step-and-ramp function. We subtract the best linear polynomial fit for each source and correct the orbital periods accordingly. For IGR J16393-4643 (top) we only use the first four points to obtain a good fit (see Section 3.1).

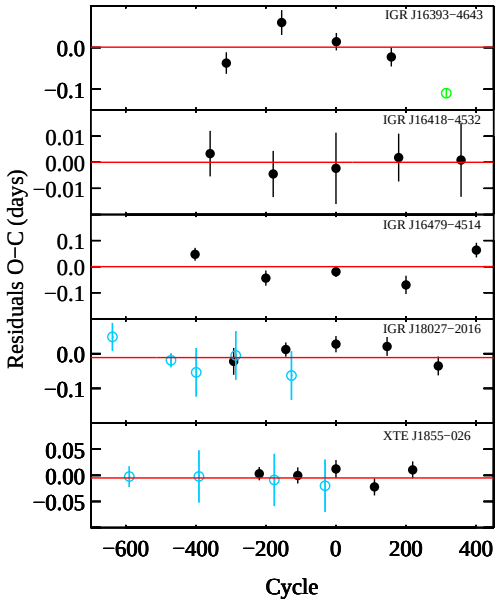

Fig. 3.— Derived $O-C$ eclipse time residuals for IGR J16393-4643 (top), IGR J16418-4532 (second panel), IGR J16479-4514 (middle), IGR J18027-2016 (fourth panel) and XTE J1855-026 (bottom) fit combined with those in the literature. We subtract the best linear polynomial fit for each source and correct the orbital periods accordingly. For IGR J16393-4643 (top) we only use the first four points to obtain a good fit (see Section 3.1).

energy band, the unabsorbed flux was found to be 9.2×10^{-11} erg cm^{-2} s^{-1} (Bodaghee et al. 2006). A proposed mass donor 2MASS J16390535-4242137 was found in the *XMM-Newton* error circle, which is thought to be an OB supergiant (Bodaghee et al. 2006). However, a precise position of the donor star obtained with *Chandra* shows this candidate to be positionally inconsistent with the X-ray source (Bodaghee et al. 2012). Using the *Spitzer* Galactic Legacy Infrared Mid-Plane Survey (GLIMPSE), Bodaghee et al. (2012) proposed that the counterpart must be a distant reddened B-type main-sequence star.

Using *INTEGRAL* and *XMM-Newton*, Bodaghee et al. (2006) found a 912.0±0.1 s modulation, which was interpreted as the neutron star rotation period. Islam et al. (2015) recently refined this to 908.79±0.01 s using *Suzaku*. A ∼3.7 day orbital period was suggested using a pulse timing analysis, although orbital periods of ∼50.2 and ∼8.1 days were not completely ruled out (Thompson et al. 2006). While various possible orbital solutions and accretion mechanisms have been proposed, orbital periods of 4.2368±0.0007 and 4.2371±0.0007 days were clearly found from data from *Swift*-BAT and *RXTE* PCA, respectively (Corbet et al. 2010). This was refined to 4.2386±0.0003 d (Corbet & Krimm 2013), also using BAT data. Islam et al. (2015) re-

cently derived an orbital period of ∼366150 s (4.24 d) with BAT, which is also consistent with the result from Corbet & Krimm (2013). The position in Corbet's diagram shows that IGR J16393-4643 is an SGXB (Corbet & Krimm 2013). Corbet & Krimm (2013) identified the presence of a possible superorbital period of ∼15 days; although with low significance.

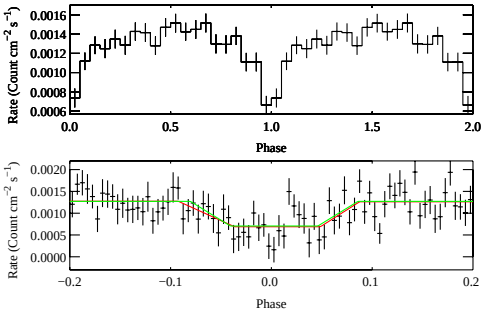

Fig. 4.— *Swift*-BAT light curve of IGR J16393-4643 in the 15–50 keV band folded on the orbital period (top) using 20 bins. T0 is defined at BMJD 55074.99, corresponding to mid-eclipse. A detailed folded light curve with 80 bins (bottom) is fit with both a symmetric "step and ramp" function (green) and asymmetric "step and ramp" function (red), which model the eclipse. The symmetric "step and ramp" function was shifted accordingly.

The BAT light curves folded on the orbital period revealed a sharp dip, which was interpreted as an eclipse (Corbet & Krimm 2013; Islam et al. 2015). With *Swift* BAT, Islam et al. (2015) constrained the eclipse half angle to be ∼17°, corresponding to a duration of ∼0.75 d (∼65.1 ks). Using the relationship between eclipse duration and stellar radius, along with the definition of the Roche-lobe from Bowers & Deeming (1984), Islam et al. (2015) calculated the allowed range of orbital inclinations of the system. Assuming a star with spectral type O9 I (Bodaghee et al. 2012), the orbital inclination was constrained to 39–57° (Islam et al. 2015). A main-sequence B-type star yields orbital inclinations between 60–77° (Bodaghee et al. 2012; Islam et al. 2015).

We derive a 4.2378±0.0004 d orbital period for IGR J16393-4643 using a DFT, which is consistent with the results from Corbet & Krimm (2013). Using an $O-C$ analysis (see Section 2.2), this is further refined to 4.23810±0.00007 d. We note that we obtain a bad fit in the mid-eclipse time between MJD 56079–56745. As a result, we only use data between MJD 53416–56078 in our $O-C$ analysis (see Figures 1–3– 3). Using the quadratic orbital change function (see Equation 4), we find the orbital period derivative to be -5±4×10^{-7} d d^{-1}, which is consistent with zero. The duration of the observed eclipse was calculated to be 31^{+6}_{-5} ks ($0.36^{+0.07}_{-0.06}$ d), yielding an eclipse half-angle of 15^{+2}_{-3}° (see Table 1). We find these to be consistent with the result from Islam et al. (2015). The source flux does not reach 0 counts cm^{-2} s^{1} in the folded light curves during eclipse (see Figure 4). We interpret this dip as an eclipse since the feature is persistent over many years of data. The rapid ingress and egress requires obscuration by clearly defined boundaries that are suggestive of an object such as the mass donor in the system (e.g. Coley et al. 2014). We discuss the nature of the non-zero flux during eclipse in Section 4.2.

We calculate the predicted eclipse half-angle Θ_e as a function of inclination angle of the system (see Figure 5). The calculation assumes a neutron star mass of 1.4 $M_\odot$, and the primary stellar masses and radii given in Table 6. We calculate the minimum inclination angle of the system, $i_{\rm min}$, that is consistent with the measured eclipse half-angle (see Table 6). We find that stars with spectral types B0 V, B0-5 III and B0 I satisfy the constraint imposed by the eclipse half-angle (see Table 6). We note that while a B5 III star satisfies the constraint imposed by the minimum value of the eclipse half-angle under the assumption that the neutron star is 1.4 $M_\odot$, this spectral type does not satisfy the eclipse half-angle for a more massive neutron star.

Since the X-ray luminosity is lower than what would be expected for Roche-lobe overflow (Kaper et al. 2004), we can attach an additional constraint assuming that the mass donor underfills the Roche-lobe radius (see Figure 6). We note that while the derived masses and radii for the spectral type B0 I from Carroll & Ostlie (2006) satisfies the eclipse half-angle, the assumed radius would be larger than the Roche-lobe radius (Eggleton

TABLE 6
PHYSICAL PARAMETERS FOR PREVIOUSLY PROPOSED MASS DONORS FOR IGR J16393-4643

Spectral Type	$M/M_\odot$	q^a	$R/R_\odot$	$R_L/R_\odot{}^b$	$i_{\min}{}^{\circ c}$
B0 III	*20*	0.070	*13*	18.5	68
B5 III	*7*	0.200	*6.3*	11.7	79
B0 V	*17.5*	0.080	*8.4*	17.5	79
B0 I	*25*	0.056	*25*[d]	20.4[d]	41

NOTE.—The values in italics are obtained from Carroll & Ostlie (2006)
[a] The mass ratio, q, is defined as M_x/M_c where M_x is the compact object and M_c is the donor star.
[b] The definition for the Roche lobe, R_L, as given in Eggleton (1983), assuming M_{NS} is $1.4\,M_\odot$.
[c] The minimum inclination angle of the system that is consistent with the measured eclipse half-angle.
[d] A B0 I classification significantly overfills the Roche-lobe and are therefore, it is excluded from our analysis.

1983). Therefore, an B0 I spectral type must be excluded (see Table 6).

3.2. IGR J16418-4532

IGR J16418-4532 is a candidate Supergiant Fast X-ray Transient (SFXT) first discovered with the *INTEGRAL* satellite by Tomsick et al. (2004) at a flux of 3×10^{-11} erg cm^{-2} s^{-1} in the 20–40 keV band. The near-infrared spectral energy distribution of the most probable Two Micron All Sky Survey (2MASS) counterpart was measured with the 3.5 m New Technology Telescope (NTT) at La Silla Observatory, Rahoui et al. (2008) found a spectral type of O8.5 I. Coleiro et al. (2013) proposed a spectral type of BN0.5 Ia based on features in the near-infrared spectrum such as Br$(7-4)$ and the emission and absorption of neutral helium. Using *XMM-Newton*, Walter et al. (2006) found a 1246±100 s modulation, which was interpreted as a neutron star rotation period. This was later refined to 1212±6 s (Sidoli et al. 2012), also using *XMM-Newton*. Recently, Drave et al. (2013) further refined the rotation period to 1209.1±0.4 s with *XMM-Newton*. A ∼3.73 d orbital period was found using data from the *Swift* BAT and the *RXTE* ASM instruments, where P_{orb} was reported as 3.753±0.004 d and 3.7389±0.0004 d, respectively (Corbet et al. 2006). Using an extended ASM dataset, Levine et al. (2011) found a 3.73886±0.00028 d period, which is consistent with the earlier result from Corbet et al. (2006). Corbet & Krimm (2013) further refined this to 3.73886±0.00014 d using BAT. A ∼14.7 d modulation was found using BAT and *INTEGRAL*, which was interpreted as a superorbital period (Corbet & Krimm 2013; Drave et al. 2013).

The ASM and BAT light curves folded on the orbital period revealed a sharp dip with near zero mean flux, which was interpreted as a total eclipse (Corbet et al. 2006). Subsequent observations of the eclipse included *Swift* X-ray Telescope (XRT) (Romano et al. 2012) and *INTEGRAL* (Drave et al. 2013). With *Swift* BAT, Romano et al. (2012) constrained the eclipse half-angle to be 0.17±0.05 of the orbital period, corresponding to a duration of 0.6±0.2 d (55±16 ks). The duration of the eclipse was found to be ∼0.75 d in the archival data set from *INTEGRAL*/IBIS, covering the time period MJD 52650–55469 (Drave et al. 2013). While the estimate in Drave et al. (2013) is significantly larger than the constraints from Romano et al. (2012), a lower limit of ∼0.583 d was found in

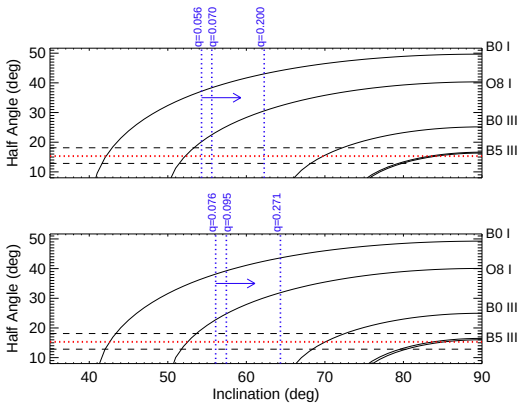

Fig. 5.— The black curves show the predicted eclipse half angle of IGR J16393-4643 as a function of inclination angle for stars with the indicated spectral types. The red and black dashed lines indicate the eclipse half angle and estimated error as measured by *Swift* BAT. We assume a neutron star mass of 1.4 $M_{\odot}$ (top) and of mass 1.9 $M_{\odot}$ (bottom) and typical masses and radii for the assumed companion spectral type (see Table 6). The blue vertical dashed lines indicate the lower limit of the inclination angle. Inclinations to the left of these correspond to stars that overfill the Roche-lobe.

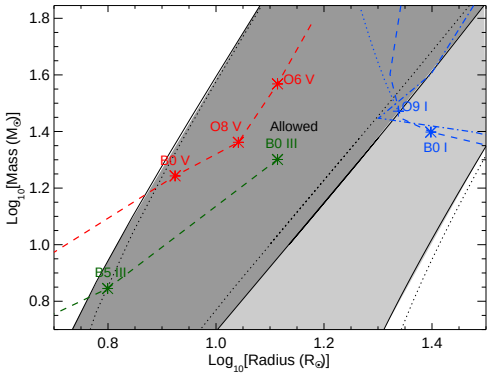

Fig. 6.— Log-log plot of stellar mass as a function of stellar radius for IGR J16393-4643. The dark shaded region indicates the allowed spectral types that satisfy the constraints imposed by both the eclipse duration and Roche-lobe size. The light shaded region only indicates spectral types that satisfy the observed eclipse duration. Stellar masses and radii are reported in Table 6. The red, green and blue lines indicate interpolations for main-sequence, giant and supergiant luminosity classes, respectively. The dashed, dotted and dash-dotted lines indicate stellar masses and radii derived from Carroll & Ostlie (2006), Martins et al. (2005) and Allen (2000), respectively.

a combined study with *INTEGRAL*/IBIS and *XMM-Newton* (Drave et al. 2013).

We derive a 3.73863±0.00015 d orbital period for IGR J16418-4532 using the fundamental peak in the power spectrum, while the first harmonic yields 3.73882±0.00011 d. Using an $O-C$ analysis (see Figures 1–3), we refine this to 3.73881±0.00002 d. Using the quadratic orbital change function (see Equation 4), we find the orbital period derivative to be $0.7\pm1.0\times10^{-7}$ d d^{-1}, which is consistent with zero. Folding the light curve on our refined orbital period (see Figure 7), we calculate the duration of the observed eclipse to be 57±1 ks (0.66±0.01 d). This yields an eclipse half-angle of $31.7^{+0.7}_{-0.8}{}^{\circ}$ (see Table 2). We note that we find the eclipse half-angle to be 31.5±0.6° assuming a symmetric step-and-ramp function. We find the eclipse properties to be consistent with the results from Romano et al. (2012) and Drave et al. (2013). Under the assumption that the mass and radius of the proposed mass donor are 31.54 $M_{\odot}$ and 21.41 $R_{\odot}$ (Martins et al. 2005), the duration of the observed eclipse is consistent with the proposed mass donor, where we find the orbital inclination to be 60–63° for an O8.5 I spectral type (see Figures 8 and 9).

Since the X-ray luminosity is lower than what would be expected for Roche-lobe overflow (Kaper et al. 2004), we can attach an additional constraint assuming that the mass donor underfills the Roche-lobe radius (see Figure 9). We note that while the derived masses and radii for the spectral types from Martins et al. (2005) satisfy the eclipse half-angle, the assumed radius would be larger than the Roche-lobe radius (Eggleton 1983). Therefore, an O8.5 I spectral type must be excluded.

TABLE 7
PHYSICAL PARAMETERS FOR PREVIOUSLY PROPOSED MASS DONORS FOR IGR J16418-4532

Spectral Type	$M/M_\odot$	q^a	$R/R_\odot$	$R_L/R_\odot{}^b$	i°
O8.5 I	*31.54*	0.044	*21.41*^{c}	20.71^c	61–63
O8.5 I	*33.90*	0.041	*22.20*^{c}	21.35^c	60–62
O9 I	*29.63*	0.047	*21.76*^{c}	20.17^c	58–60
O9 I	*31.95*	0.044	*22.60*^{c}	20.82^c	57–59

NOTE.—The values in italics are obtained from Martins et al. (2005).
[a] The mass ratio, q, is defined as M_x/M_c where M_x is the compact object and M_c is the donor star.
[b] The definition for the Roche lobe, R_L, as given in Eggleton (1983), assuming M_{NS} is $1.4\,M_\odot$.
[c] These spectral types significantly overfill the Roche-lobe and are therefore excluded from our analysis.

3.3. IGR J16479-4514

IGR J16479-4514 is an intermediate SFXT, which has been proposed to host either an O8.5 I (Chaty et al. 2008; Rahoui et al. 2008) or a O9.5 Iab (Nespoli et al. 2008) mass donor. First discovered by the *INTEGRAL* satellite in 2003 August (Molkov et al. 2003), the fluxes in the 18–25 keV and 25–50 keV energy bands were found to be ∼12 mCrab and ∼8 mCrab, respectively. The flux was later shown to increase by a factor of ∼2 on 2003 August 10 (Molkov et al. 2003). Using *Swift* BAT data, Jain et al. (2009) found the presence of a 3.319±0.001 day modulation, which was interpreted as the orbital period. A 3.3193±0.0005 day modulation was independently found by Romano et al. (2009) also using BAT. Corbet & Krimm (2013) found the orbital period to be 3.3199±0.0005 d, which is consistent with the results from Jain et al. (2009) and Romano et al. (2009). The presence of a 11.880±0.002 d superorbital period was found by Corbet & Krimm (2013) using BAT. Drave et al. (2013) reported a 11.891±0.002 d superorbital period using *INTEGRAL*, confirming the result. No pulse period has been identified.

The BAT light curves folded on the orbital period revealed a sharp dip, which was interpreted as an eclipse with a proposed duration of ∼52 ks (Jain et al. 2009). This confirmed an earlier *XMM-Newton* observation where a decay from a higher to lower flux state was interpreted as the ingress of an eclipse (Bozzo et al. 2009). A 2012 *Suzaku* observation covered ∼80 percent of the orbital cycle of IGR J16479-4514, where temporal and spectral properties were analyzed during eclipse and out-of-eclipse (Sidoli et al. 2013). Since the ingress of the eclipse was not covered in *Suzaku* observation, the exact duration of the eclipse could only be constrained to 46–143 ks (0.53–1.66 d) (Sidoli et al. 2013).

Using a DFT, we derive the orbital period of IGR J16479-4514 to be 3.31998±0.00014 d. We refine this to 3.31961±0.00004 d using an $O-C$ analysis (see Figures 1–3) and fold the light curve on our refined orbital period to calculate the eclipse half-angle (see Figure 10). Using the quadratic orbital change function (see Equation 4), we find the orbital period derivative to be $3\pm2\times10^{-7}$ d d^{-1}, which is consistent with zero. We calculate the duration of the observed eclipse to be 52±3 ks (0.60±0.03 d), which is consistent with results from Jain et al. (2009). This yields an eclipse half-angle of $31.9^{+0.9}_{-1.3}{}^\circ$ (see Table 1). Using values from Martins et al. (2005) for the masses and radii of the proposed spectral type of the mass donor, the duration of the observed eclipse is consistent

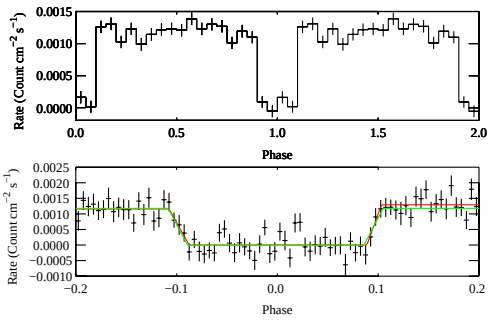

Fig. 7.— *Swift*-BAT light curve of IGR J16418-4532 in the 15–50 keV band folded on the orbital period (top) using 20 bins. T0 is defined at BMJD 55087.721, corresponding to mid-eclipse. A detailed folded light curve with 80 bins (bottom) is fit with both a symmetric "step and ramp" function (green) and asymmetric "step and ramp" function (red), which model the eclipse. The symmetric "step and ramp" function was shifted accordingly.

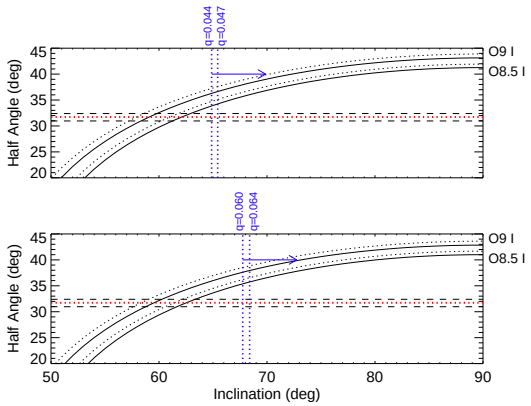

Fig. 8.— The black curves show the predicted eclipse half angle of IGR J16418-4532 as a function of inclination angle for stars with the indicated spectral types. The red and black dashed lines indicate the eclipse half angle and estimated error as measured by *Swift* BAT. We assume a neutron star mass of 1.4 $M_\odot$ (top) and of mass 1.9 $M_\odot$ (bottom) and typical masses and radii for the assumed companion spectral type (see Table 7). The blue vertical dashed lines indicate the lower limit of the inclination angle. Inclinations to the left of these correspond to stars that overfill the Roche-lobe.

with the proposed mass donor (see Figures 11), where we find the orbital inclination to be 54–58° or 47–51° for a O8.5 I or O9.5 Iab spectral type, respectively (see Table 8). While the previously preposed spectral types satisfy the eclipse half-angle, we note that the radius of the proposed spectral type is larger than the Roche-lobe (Eggleton 1983). Therefore, the previously proposed O8.5 I or O9.5 Iab spectral types must be excluded (see Figure 12). Sidoli et al. (2013) proposed a mass donor with mass $\sim$35 $M_\odot$ and radius $\sim$20 $R_\odot$, which could satisfy the constraints imposed by the Roche-lobe radius.

3.4. IGR J18027-2016 (=SAX J1802.7-2017)

IGR J18027-2016 (=SAX J1802.7-2017) is an SGXB, which has been proposed to host either a B1 Ib (Torrejón et al. 2010) or B0-B1 I (Mason et al. 2011) mass donor. First detected with *BeppoSAX* in 2001 September (Augello et al. 2003), the average flux in the 0.1–10 keV energy band was found to be 3.6×10^{-11} ergs cm^{-2} s^{-1}. Pulse-timing analysis suggested a $\sim$4.6 day orbital period (Augello et al. 2003), which was later refined to 4.5696±0.0009 days using *INTEGRAL* (Hill et al. 2005). Combining the mid-eclipse times derived in Augello et al. (2003) and Hill et al. (2005) with later observations with *Swift* BAT and *INTEGRAL* in an $O-C$ analysis, the orbital period was further refined to 4.5693±0.0004 d (Jain et al. 2009). Fitting a quadratic model to the derived mid-eclipse times, a period derivative of $(3.9\pm1.2)\times10^{-7}$ d d^{-1} was found (Jain et al. 2009). Using *INTEGRAL*, Falanga et al. (2015) recently refined the orbital period and period derivative to 4.5697±0.0001 d and $(2.1\pm3.6)\times10^{-7}$ d d^{-1}, respectively. Augello et al. (2003) found the presence of a $\sim$139.6 s modulation using *BeppoSAX*, which they interpeted as the neutron star rotation period. Hill et al. (2005) found the pulse period using *XMM-Newton* to be 139.61±0.04 s, which is consistent with an earlier result from Augello et al. (2003). However, no evidence for superorbital modulation was found

Table 8
Physical Parameters for Previously Proposed Mass Donors for IGR J16479-4514

Spectral Type	$M/M_\odot$	q^a	$R/R_\odot$	$R_L/R_\odot{}^b$	i°
O8.5 I	*31.54*	0.044	*21.41*^{c}	19.13^c	55–58
O8.5 I	*33.90*	0.041	*22.20*^{c}	19.73^c	54–56
O9.5 I	*27.83*	0.050	*22.11*^{c}	18.14^c	48–51
O9.5 I	*30.41*	0.046	*23.11*^{c}	18.84^c	47–49

Note.—The values in italics are obtained from Martins et al. (2005).
[a] The mass ratio, q, is defined as M_x/M_c where M_x is the compact object and M_c is the donor star.
[b] The definition for the Roche lobe, R_L, as given in Eggleton (1983), assuming M_{NS} is $1.4\,M_\odot$.
[c] These spectral types significantly overfill the Roche-lobe and are therefore excluded from our analysis.

(Corbet & Krimm 2013).

Augello et al. (2003) derived the epoch of the NS superior conjuction to occur during the first 50 ks of an observation where IGR J18027-2016 was undetected. Since the epoch of superior conjuction corresponds to a time where the mid-eclipse is expected to occur, Augello et al. (2003) suggested the presence of a possible eclipse with a half-duration of 0.47±0.10 days. Hill et al. (2005) and Jain et al. (2009) later confirmed this result where the eclispe half-angle was found to be 0.61±0.08 radians (34.9±4.6 °) and ∼0.604 radians (∼34.6 °), respectively. Falanga et al. (2015) recently refined the eclipse half-angle to 31±2 ° using *INTEGRAL*.

Pulse-timing and radial velocity curves have helped place constraints on the physical properties on both the donor star as well as the compact object. Using a pulse-timing analysis with *BeppoSAX* and *XMM-Newton*, the projected semi-major axis of the neutron star was found to be 68±1 lt-s (Hill et al. 2005). Assuming a $1.4\,M_\odot$ neutron star, Hill et al. (2005) constrained the mass and radius of the mass donor star to 18.8–$29.3\,M_\odot$ and 14.7–$23.4\,R_\odot$, respectively. Using *Swift* BAT and *INTEGRAL*, Jain et al. (2009) further constrained the radius of the donor star to 16.4–$24.7\,R_\odot$. The mass donor was observed between 2010 May 26 and 2010 September 8 (MJD 55342–55447) with the *European Southern Observatory Very Large Telescope* (*ESO VLT*, Mason et al. 2011). The semi-amplitude of the radial velocity of the mass donor, K_O, was found to be 23.8±3.1 km s^{-1} (Mason et al. 2011). Since the projected semi-major axis of the neutron star can be expressed in terms of a radial velocity semi-amplitude, K_X, the ratio between the masses of the compact object and the mass donor can be calculated according to Equation 2 in Ash et al. (1999). Mason et al. (2011) found the mass ratio, q, to be 0.07±0.01. Using the mass ratio and the eclipse half-angle measured in Hill et al. (2005), the mass and radius of the donor star were refined to values between $18.6\pm0.8\,M_\odot$ and $16.8\pm1.5\,R_\odot$ at edge-on inclinations to $21.8\pm2.4\,M_\odot$ and $19.8\pm0.7\,R_\odot$ where the donor star fills the Roche-lobe (Mason et al. 2011). The mass of the compact object was constrained to be between 1.36±0.21 and $1.58\pm0.27\,M_\odot$ in the two limits. The large error on the estimate of the eclipse half-angle from Hill et al. (2005) contributes significantly to the uncertainties on these measurements. Using a similar analysis with *INTEGRAL*, Falanga et al. (2015) constrained the mass of the neutron star to $1.6\pm0.3\,M_\odot$.

We derive a 4.57022±0.00013 d orbital period

TABLE 9
SYSTEM PARAMETERS FOR IGR J18027-2016

Parameter	Value
$P_{\rm orb}$ [a]	4.56993±0.00003 d
$P_{\rm pulse}$ [b]	139.61±0.04 s
$a_{\rm x}\ sini$ [b]	68±1 lt-s
$K_{\rm o}$ [c]	23.8±3.1 km s^{-1}
$T_{\rm mid}$	BMJD 55083.82±0.01
$f(M)$ [b]	16±1 $M_{\odot}$
q [c]	0.07±0.01
$\Theta_{\rm e}$	34±2°
$M_{\rm donor}$	18.6±0.9–19.4±0.9 $M_{\odot}$
$R_{\rm donor}$	17.4±0.9–$19.5^{+0.8}_{-0.7}$ $R_{\odot}$
a	31.4–33.2 $R_{\odot}$
$M_{\rm NS}$	1.37±0.19–1.43±0.20 $M_{\odot}$
i	73.3–90°

NOTE.—[a] The orbital period is refined using an $O-C$ analysis.
[b] The pulse period, projected semi-major axis and mass function are given in Hill et al. (2005).
[c] The semi-amplitude of the radial velocity of the mass donor and mass ratio are given in Mason et al. (2011).

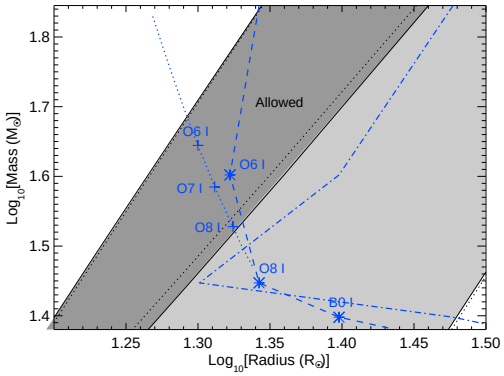

Fig. 9.— Log-log plot of stellar mass as a function of stellar radius for IGR J16418-4532. The dark shaded region indicates the allowed spectral types that satisfy the constraints imposed by both the eclipse duration and Roche-lobe size. The light shaded region only indicates spectral types that satisfy the observed eclipse duration. Stellar masses and radii are reported in Table 7. The dashed, dotted and dash-dotted lines indicate stellar masses and radii derived from Carroll & Ostlie (2006), Martins et al. (2005) and Allen (2000), respectively.

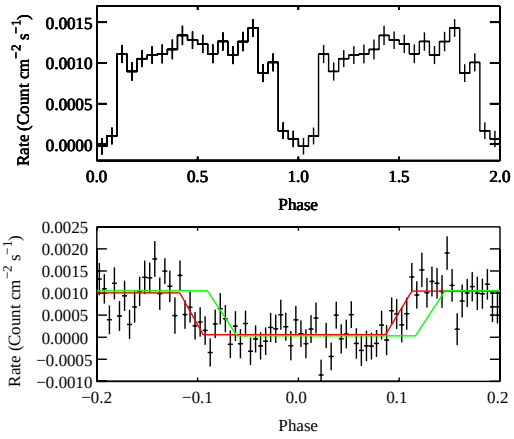

Fig. 10.— *Swift*-BAT light curve of IGR J16479-4514 in the 15–50 keV band folded on the orbital period (top) using 20 bins. T0 is defined at BMJD 55081.57, corresponding to mid-eclipse. A detailed folded folded light curve with 80 bins (bottom) is fit with both a symmetric "step and ramp" function (green) and asymmetric "step and ramp" function (red), which models the eclipse. The symmetric "step and ramp" function was shifted accordingly.

for IGR J18027-2016 using a DFT, which is consistent with the results from Hill et al. (2005). Using an $O-C$ analysis (see Figures 1–3), we refine this to 4.56993±0.00003 d. Using the quadratic orbital change function (see Equation 4), we find the orbital period derivative to be $0.2\pm1.1\times10^{-7}$ d d^{-1}, which is consistent with zero. Folding the light curve on our refined orbital period(see Figure 13), we measure the duration of the observed eclipse to be 74±4 ks (0.85±0.05 d). We find the eclipse half-angle to be 34±2° (see Table 1). Since the X-ray luminosity of IGR J18027-2016 is modest, we again attach the constraint that the donor star underfills the Roche-lobe (see Figures 14 and 15). This constrains the mass and radius of the donor star as well as the mass of the neutron star (see Figure 15). Using the eclipse half-angle and the expression for the mass donor when the mass ratio is known (Eq.4; Mason et al. 2011), we calculate the donor star mass and radius as well as mass of the compact object. We find the mass and radius of the donor star to be 18.6±0.9 $M_\odot$ and 17.4±0.9 $R_\odot$ and 19.4±0.9 $M_\odot$ and $19.5^{+0.8}_{-0.7}$ $R_\odot$ in the two limits (see Table 9). In the allowed limits, we constrain the mass of the neutron star to between 1.37±0.19 $M_\odot$ and 1.43±0.20 $M_\odot$ (see Table 9). While our results are in agreement with calculations in Mason et al. (2011), we note that the error estimate is only marginally improved in our analysis. The driving factor on the error estimate of the neutron star mass is the uncertainty of ∼13% on the semi-amplitude of the radial velocity of the donor star as reported in Mason et al. (2011).

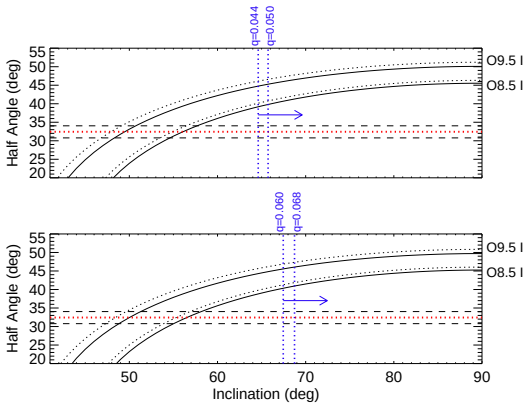

Fig. 11.— The black curves show the predicted eclipse half angle of IGR J16479-4514 as a function of inclination angle for stars with the indicated spectral types. The red and black dashed lines indicate the eclipse half angle and estimated error as measured by *Swift* BAT. We assume a neutron star mass of 1.4 $M_\odot$ (top) and of mass 1.9 $M_\odot$ (bottom) and typical masses and radii for the assumed companion spectral type (see Table 8). The blue vertical dashed lines indicate the lower limit of the inclination angle. Inclinations to the left of these correspond to stars that overfill the Roche-lobe.

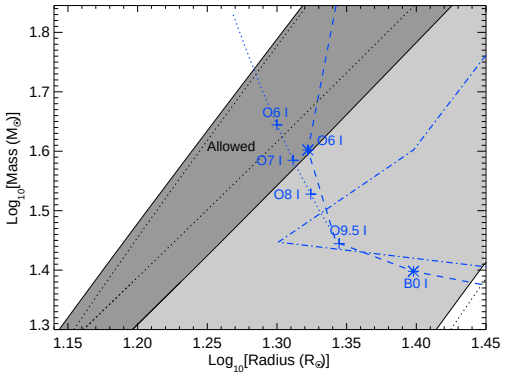

Fig. 12.— Log-log plot of stellar masses as a function of stellar radius for IGR J16479-4514. The light shaded region indicates the allowed spectral types that satisfy the observed eclipse. The dark shaded region indicates the spectral types where both the eclipse duration and Roche-lobe radius constraints are satisfied. Stellar masses and radii are reported in Table 8. The dashed, dotted and dash-dotted lines indicate stellar masses and radii derived from Carroll & Ostlie (2006), Martins et al. (2005) and Allen (2000), respectively.

3.5. XTE J1855-026

XTE J1855-026 is an SGXB discovered during *RXTE* scans along the Galactic plane (Corbet et al. 1999). Through 11 scanning observations of the Scutum arm, the 2–10 keV flux of XTE J1855-026 varied from an upper limit of 10 counts s^{-1} to 136±15 counts s^{-1} (Corbet et al. 1999). Using the *RXTE* Proportional Counter Array (PCA), Corbet et al. (1999) found a 361.1±0.4 s modulation, which was interpreted as the neutron star rotation period. Corbet & Mukai (2002) later refined the pulse period to 360.741±0.002 s with the PCA. An analysis using the *RXTE* All-sky Monitor (ASM) revealed the presence of a 6.0724±0.0009 d modulation, which is interpreted as the orbital period (Corbet & Mukai 2002). Using an $O-C$ analysis with *INTEGRAL*, Falanga et al. (2015) recently refined this to 6.07415±0.00008 d. No significant orbital period derivative was found using the quadratic orbital change function (Falanga et al. 2015). This places XTE J1855-026 in the wind-fed supergiant region of the Corbet diagram (Corbet 1986). Corbet & Mukai (2002) constrained the eccentricity of XTE J1855-026 to e≤0.04 using pulse-timing analysis. The projected semi-major axis of the neutron star was found to be 82.8±0.8 lt-s for a circular orbit and 80.5±1.4 lt-s for the eccentric solution (Corbet & Mukai 2002). In this section, we consider the scenario where the orbit is circular. We calculate constraints on the mass and radius of the donor star in the more complicated scenario where the orbit is considered to have a modest eccentricity in Section 4.3. Using optical and near-infrared spectroscopy obtained with the William Herschel Telescope (WHT), Negueruela et al. (2008) found the mass donor to be a supergiant with spectral type B0 Iaep.

The light curves folded on the orbital period reveal a sharp dip, which was interpreted as an eclipse with a total phase duration of 0.198–0.262 (Corbet & Mukai 2002). The phase duration corresponded to an eclipse half-angle $36^\circ \leq \Theta_e \leq 47^\circ$.

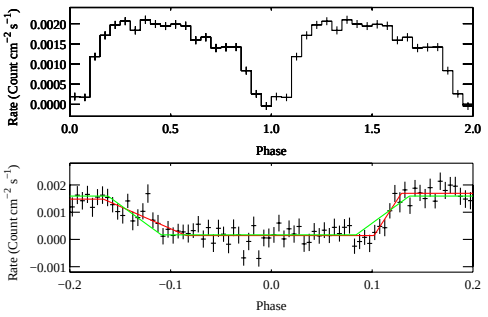

Fig. 13.— *Swift*-BAT light curve of IGR J18027-2016 in the 15–50 keV band folded on the orbital period (top) using 20 bins. T0 is defined at BMJD 55083.82±0.01, corresponding to mid-eclipse. A detailed folded light curve with 80 bins (bottom) is fit with both a symmetric "step and ramp" function (green) and asymmetric "step and ramp" function (red), which model the eclipse. The symmetric "step and ramp" function was shifted accordingly.

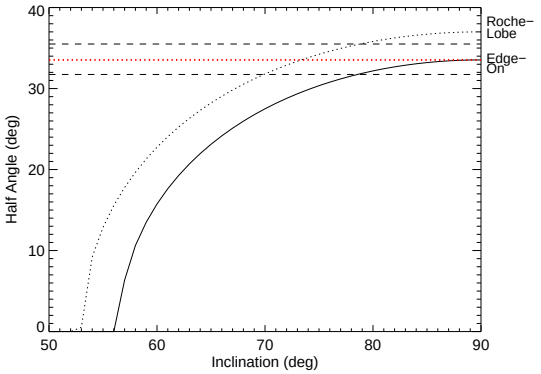

Fig. 14.— The black curves show the predicted eclipse half angle of IGR J18027-2016 as a function of inclination angle for stars with the indicated spectral types. The red and black dashed lines indicate the eclipse half angle and estimated error as measured by *Swift* BAT.

The eclipse duration was found to be 93±3 ks (1.08±0.03 d) in the archival *INTEGRAL* data set (Falanga et al. 2015), corresponding to an eclipse half-angle of 32±1°. This measurement is somewhat lower than result from Corbet & Mukai (2002).

Optical radial velocity curves recently obtained with the *Isaac Newton Telescope (INT)*, the *Liverpool Telescope (LT)* and the *WHT* help place additional constraints on the components of the system (González-Galán 2015). The semi-amplitude of the radial velocity of the donor star was found to be 26.8±8.2 km s^{-1}. Expressing the projected semi-major axis of the neutron star as a radial velocity semi-amplitude, González-Galán (2015) found the ratio between the masses of the components of the system to be 0.09±0.03 and notes that a large eccentricity of ∼0.4–0.5 was found in the optical orbital solutions. This strongly contrasts with the X-ray orbital solution reported in Corbet & Mukai (2002), suggesting that caution must be taken in interpreting the optical orbital solutions. González-Galán (2015) refined the spectral type of the mass donor to a BN0.2 Ia supergiant and found the mass and radius of the donor star to be $13^{+19}_{-7}\,M_\odot$ and $27^{+21}_{-10}\,R_\odot$, respectively.

We derive a 6.07411±0.00014 d orbital period for XTE J1855-026 using the fundamental peak in the power spectrum. Using an $O-C$ analysis (see Figures 1–3), we refine this to 6.07413±0.00004 d and fold the light curve on the refined orbital period to calculate the eclipse half-angle (see Figures 16 and 17). We calculate the duration of the observed eclipse to be 98±2 ks (1.13±0.02 d), yielding an eclipse half-angle of 33.6±0.7 degrees (see Table 10). This indicates that our derived eclipse duration is somewhat less than the result from Corbet & Mukai (2002) and is consistent with the measurement in Falanga et al. (2015).Using the quadratic orbital change function (see Equation 4), we find the orbital period derivative to be $0.0\pm0.5\times10^{-7}$ d d^{-1}, which is consistent with zero.

Since the upper limits of the stellar mass and radius are constrained by the orbital inclination where the Roche lobe is just filled, we again attach constraints on the mass and radius of the donor star as well as the mass of the compact object. We find the inclination where the donor star fills the Roche lobe to be 76.4°. The stellar mass and radius of the donor star are found to be 19.6±1.1 $M_\odot$ and 21.5±0.5 $R_\odot$ and 20.2±1.2 $M_\odot$

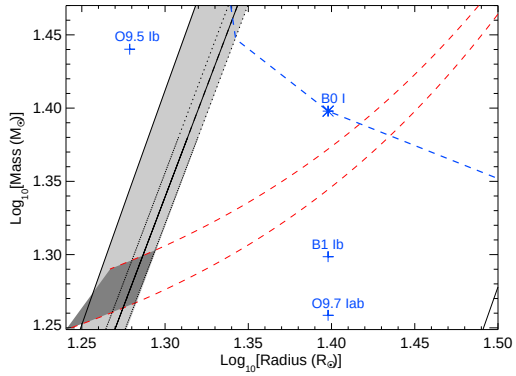

Fig. 15.— Log-log plots of stellar masses as a function of stellar radii for IGR J18027-2016. The shaded region indicates the allowed spectral types to satisfy the observed eclipse duration and pulse-timing constraints. Stellar masses and radii are reported in Table 9. Stars and crosses indicate the spectral types according to Carroll & Ostlie (2006) and Lefever et al. (2007), respectively.

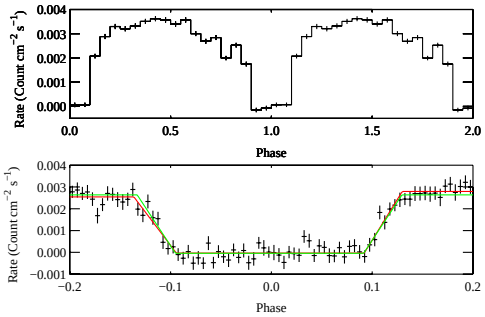

Fig. 16.— *Swift*-BAT light curve of XTE J1855-026 in the 15–50 keV band folded on the orbital period (top) using 20 bins. T0 is defined as MJD 55079.0685, corresponding to mid-eclipse. A detailed folded folded light curve with 80 bins (bottom) is fit with both a symmetric "step and ramp" function (blue) and asymmetric "step and ramp" function (red), which models the eclipse.

and $23.0\pm0.5\,R_\odot$ in the two limits (see Table 18). We find the mass of the neutron star to be between $1.77\pm0.55\,M_\odot$ and $1.82\pm0.57\,M_\odot$ (see Table 18), where the driving factor on the large error estimate is the uncertainty of ∼31% on the radial velocity semi-amplitude of the donor star as reported in González-Galán (2015).

4. Discussion

We discuss our findings of IGR J16393-4643, IGR J16418-4532, IGR J16479-4514, IGR J18027-2016 and XTE J1855-055. The radii for the previously proposed spectral types in IGR J16418-4532 and IGR J16479-4514 would significantly overfill the Roche-lobe, which suggests an earlier spectral type. Below, we discuss in detail the nature of the mass donors in each system, mechanisms that could result in the residual emission observed in IGR J16393-4643 and comment on the nature of the eclipse profiles.

4.1. What is the nature of the mass donors in each system?

4.1.1. IGR J16393-4643

Our results show that stars with spectral type B0 V and B0-5 III satisfy the constraints imposed by the eclipse half-angle as well as the Roche-lobe (see Section 3.1). While some supergiant stars such as a B0 I satisfy the eclipse half-angle, the required radius would be larger than the Roche-lobe. We calculated the Roche-lobe radius for stars of spectral type B0 I to be $18.5\,R_\odot$. This is clearly smaller than the radii reported in Carroll & Ostlie (2006) and Allen (2000), which are $25\,R_\odot$ and $30\,R_\odot$, respectively (see Table 6). Since the radius for this proposed supergiant is too large to satisfy the constraint imposed by the Roche-lobe, we suggest that if the donor star is a supergiant then it must be a slightly earlier spectral type.

IGR J16393-4643 was observed in the near-infrared on 2004 July 9 (MJD 53195.3) using the 3.5 m New Technology Telescope (NTT) at La Silla Observatory (Chaty et al. 2008). While Chaty et al. (2008) conclude that the spectral type of the donor star is BIV-V based on the spectral features and spectral energy distribution (SED),

TABLE 10
SYSTEM PARAMETERS FOR XTE J1855-026

Parameter	Value
$P_{\rm orb}{}^a$	6.07413±0.00004 d
$P_{\rm pulse}{}^b$	360.741±0.002 s
$\dot{P}_{\rm pulse}{}^b$	1.5±3.6 s s^{-1}×10^{-8}
$a_{\rm x}\ sini^b$	82.8±0.8 lt-s
$K_{\rm o}{}^c$	26.8±8.2 km s^{-1}
$T_{\rm mid}$	MJD 55079.07±0.01
$f(M)^b$	16.5±0.5 $M_\odot$
q^c	0.09±0.03
$\Theta_{\rm e}$	33.6±0.7°
$M_{\rm donor}$	19.6±1.1–20.2±1.2 $M_\odot$
$R_{\rm donor}$	21.5±0.5–23.0±0.5 $R_\odot$
a	38.9–39.2 $R_\odot$
$M_{\rm NS}$	1.77±0.55 $M_\odot$–1.82±0.57 $M_\odot$
i	76.4–90°

NOTE.—[a] The orbital period is refined using an $O-C$ analysis.
[b] The pulse period, derivative of the pulse period, projected semi-major axis and mass function are given in Corbet & Mukai (2002).
[c] The semi-amplitude of the radial velocity of the mass donor and mass ratio are given in González-Galán (2015).

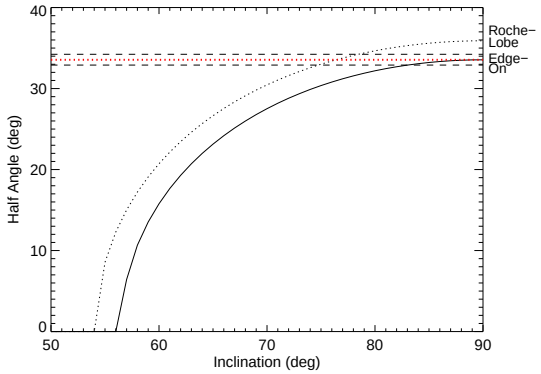

Fig. 17.— The black curves show the predicted eclipse half angle of XTE J1855-026 as a function of inclination angle for stars with the indicated spectral types. The red and black dashed lines indicate the eclipse half angle and estimated error as measured by *Swift* BAT.

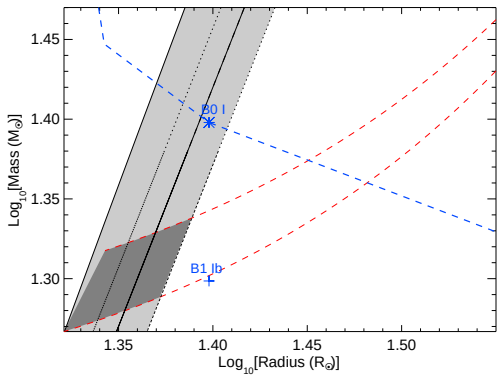

Fig. 18.— Log-log plots of stellar masses as a function of stellar radii for XTE J1855-026. The shaded region indicates the allowed spectral types to satisfy the observed eclipse duration, pulse-timing and optical radial velocity constraints. Stellar masses and radii are reported in Table 10. Stars and crosses indicate the spectral types according to Carroll & Ostlie (2006) and Lefever et al. (2007), respectively.

we note that Nespoli et al. (2008) proposed the donor star to be a K or M supergiant using the same SED. Furthermore, observations with the *Chandra* observatory show that the previously proposed counterpart is positionally inconsistent with the X-ray source (Bodaghee et al. 2012). Using the GLIMPSE survey, Bodaghee et al. (2012) proposed that the counterpart must be a distant reddened B-type star.

4.1.2. IGR J16418-4532

Our results show that while the derived masses and radii for the previously proposed spectral types satisfy the eclipse half-angle (see Table 7), the radius would be larger than the Roche-lobe size (Eggleton 1983). An O8 I star has a mass of $28\,M_{\odot}$ according to Carroll & Ostlie (2006) and Allen (2000). We find the maximum radius for a $28\,M_{\odot}$ star to satisfy the constraint imposed by the Roche-lobe to be $18.2\,R_{\odot}$. This is clearly smaller than the radii reported in Carroll & Ostlie (2006) and Allen (2000), which are $22\,R_{\odot}$ and $20\,R_{\odot}$, respectively (see Table 7). Since the radius for each proposed spectral type is too large to satisfy the constraint imposed by the Roche-lobe, it is our contention that the donor must be an earlier spectral type.

We find that spectral classes O7.5 I and earlier satisfy the constraint imposed by the Roche-lobe radius (see Table 11). The ratio between the radius of the donor star and that of the Roche-lobe, β, is found to exceed 0.9, which is consistent with other HMXBs that host supergiants (Joss & Rappaport 1984). Transitional Roche-lobe accretion has been proposed in IGR J16418-4532 where a fraction of the mass transfer is due to a focused wind (Sidoli et al. 2012). A focused wind or accretion stream requires a mass donor that nearly fills the Roche-lobe. If this is the case, we would expect variations in the mass accretion rate that would be attributable to a focused wind or accretion stream (Blondin & Owen 1997). This mechanism would lead to large variability in the X-ray intensity and could be observed in folded-light curves as well as hardness-intensity diagrams. Large intensity swings on the order of ∼100 were observed in both *Swift* and *XMM-Newton* observations of IGR J16418-4532 (Sidoli et al. 2012; Drave et al. 2013).

Near-infrared spectral features previously led to a spectral classification of either a late O-type supergiant (Chaty et al. 2008) or a BN0.5 Ia (Coleiro et al. 2013). We note the presumed

TABLE 11
POSSIBLE PARAMETERS OF CANDIDATE DONOR STARS FOR IGR J16418-4532

Spectral Type	$M/M_\odot$	q	$R/R_\odot$	$R_L/R_\odot$[a]	R_L/R	M_V	$(J-K)_0$[a]	$E(J-K)$[a]	i°[b]	d_{sun}[c] (kpc)	d_{sun}[d] (kpc)
O6 Ia	44.10	0.032	19.95	23.85	0.84	*-6.38*	-0.21	2.60	77–81	11.9	11.9
O6.5 Ia	41.20	0.034	20.22	23.18	0.87	*-6.38*	-0.21	2.60	73–76	12.0	12.1
O7 Ia	38.44	0.036	20.49	22.52	0.91	*-6.38*	-0.21	2.60	70–73	12.0	12.3
O7.5 Ia	36.00	0.039	20.79	21.90	0.95	*-6.38*	-0.21	2.60	67–69	12.0	12.4
O8 Ia	33.72	0.042	21.10	21.31	0.99	*-6.38*	-0.21	2.60	64–66	11.9	12.6

NOTE.—Possible Parameters of Candidate Donor Stars.
[a] The value for $(J-K)_0$ was calculated using $(J-H)_0$ and $(H-K)_0$ published in Martins & Plez (2006). $E(J-K)$ is found by subtracting $(J-K)_0$ from the observed $J-K$
[b] The range of inclination angles of the system consistent with the measured eclipse half-angle.
[c] The distance the object is from the Sun using the distance modulus.
[d] The distance the object is from the Sun using the radius to distance ratio derived from spectral energy distribution. The radius to distance ratio is found to be 3.77×10^{-11} (Chaty et al. 2008).

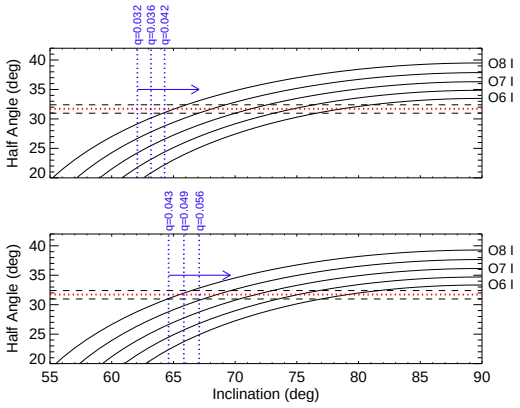

Fig. 19.— The black curves show the predicted eclipse half angle as a function of inclination angle for stars with the candidate spectral types for IGR J16418-4532. The red and black dashed lines indicate the eclipse half angle and estimated error as measured by *Swift* BAT. We assume a neutron star mass of $1.4\,M_\odot$ (top) and of mass $1.9\,M_\odot$ (bottom) and typical masses and radii for the assumed companion spectral type (see Table 12). The blue vertical dashed lines indicate the lower limit of the inclination angle. Inclinations to the left of these correspond to stars that overfill the Roche-lobe.

radius of both spectral types overfills the Roche-lobe, which shows that the proposed spectral classifications are incorrect. The spectral type of the mass donor places an additional constraint on the source distance. Under the assumption that the K-band magnitude (m_K) and extinction in the V-band (A_V) are magnitudes 11.48 and 14.5 for an O8.5 I classification, (Rahoui et al. 2008) found the distance of the source to be ∼13 kpc. Converting A_V to A_K using Table 3 in Rieke & Lebofsky (1985), we confirm the calculations for the distance of IGR J16418-4532 in Rahoui et al. (2008) using the distance modulus. The distance of IGR J16418-4532 assuming the aforementioned spectral types are reported in Table 11 using the values for M_V obtained from Wegner (2006) and Martins & Plez (2006). We also use the radius to distance ratio from the near-infrared spectral energy distribution (SED) measurements reported in (Rahoui et al. 2008) together with our eclipse measurements to estimate the distance of IGR J16418-4532. We find the distance to be between 11.9–12.6 kpc, which is slightly smaller than that reported in Rahoui et al. (2008) for an O8 I star.

IGR J16418-4532 is a heavily absorbed SFXT where the observed N_H, measured to be between $3.9^{+1.2}_{-0.9}\times10^{22}$ atoms cm^{-2} and $7\pm2\times10^{22}$ atoms cm^{-2} (Romano et al. 2012), exceeds the val-

ues reported by the Leiden/Argentine/Bonn survey (Kalberla et al. 2005) and in the review by Dickey & Lockman (1990), which are 1.59×10^{22} and 1.88×10^{22} atoms cm^{-2}, respectively. Since the measured $N_{\rm H}$ was found to be in excess of the Galactic H I, determining the interstellar fraction of $N_{\rm H}$ is problematic and the value in Rahoui et al. (2008) for the extinction cannot be verified without the presence of systematic error.

We compare the observed value of the $J-K$ color of 2.39[3] with the intrinsic $(J-K)_0$ for the proposed mass donors (see Table 11). Calculating the difference between the observed $J-K$ and the intrinsic $(J-K)_0$, we find the reddening values $E(J-K)$ for each proposed spectral type for the mass donor (see Table 11). We calculate the reddening in the $B-V$ band, $E(B-V)$, using Equation 1 in Güver & Oumlzel (2009) and the extinction in the V-band ($A_{\rm V}$) (Rahoui et al. 2008). Converting $E(B-V)$ to $E(J-K)$ using Table 3 in Rieke & Lebofsky (1985), we find $E(J-K)$ to be 2.45. While this is slightly lower than what would be expected for late O supergiant spectral types (see Table 11), the presence of systematic error described above prevents an exact calculation.

These results show that stars with spectral type O7.5 I and earlier satisfy the constraints imposed by both the duration of the eclipse and the Roche-lobe (see Figure 19). Since the measured $N_{\rm H}$ is largely in excess of interstellar values measured by Kalberla et al. (2005) and Dickey & Lockman (1990), determining what fraction of $N_{\rm H}$ is interstellar in origin is problematic. We find measurements such as the distance to be consistent with the distances determined by Rahoui et al. (2008). Given our measurements, spectral types near O7.5 I are reasonable. By constraining this type of star, we solved the first part of a three part problem. The remaining pieces include pulse-timing measurements which can be done in the X-ray and radial velocity measurements in the near-infrared.

4.1.3. IGR J16479-4514

Our results show that while the expected masses and radii for the previously proposed spectral types for IGR J16479-4514 satisfy the eclipse half-angle (see Table 8), the implied radius would be larger than the Roche-lobe radius (Eggleton 1983). This is similar to the situation observed in IGR J16418-4532, which we describe in Section 4.1.2. We calculate the Roche-lobe radius for stars of spectral types O8.5 I and O9.5 Iab to be $19.1\,R_\odot$ and $18.1\,R_\odot$, respectively (see Table 8). Since the radius for each proposed spectral type is too large to satisfy the constraint imposed by the Roche-lobe (see Table 8), we suggest that the donor must be a slightly earlier spectral type.

We find that spectral classes O7 I and earlier satisfy the Roche-lobe constraint (see Table 12). The ratio between the radius of the donor star and that of the Roche-lobe, β, is found to exceed 0.9, which is consistent with other HMXBs that host supergiants (Joss & Rappaport 1984). Transitional Roche-lobe has been proposed in IGR J16479-4514 (Sidoli et al. 2013), which requires a mass donor that nearly fills the Roche-lobe. Sidoli et al. (2013) found phase-locked flares were found in their observation of IGR J16479-4514. Sidoli et al. (2013) attributes the physical mechanism responsible for these flares which are spaced 0.2 in phase as large-scale structures in the wind.

Using near-infrared spectral features, Chaty et al. (2008) previously determined the spectral classification of the donor star to be a late O-type supergiant (Chaty et al. 2008). The donor spectral type places an additional constraint on the distance of IGR J16479-4514. The K-band magnitude ($m_{\rm K}$) and the extinction in the V-band ($A_{\rm V}$) are found to be 9.79 and 18.5 (Rahoui et al. 2008). Additionally, the R_*/D_* ratio was found to be 1×10^{-10} (Chaty et al. 2008). Using this information, the minimum distance of IGR J16479-4514 was found to be $\sim$4.9 kpc (Chaty et al. 2008). Converting $A_{\rm V}$ to $A_{\rm K}$ using Table 3 in Rieke & Lebofsky (1985), we find $A_{\rm K}$ to be 2.07 and confirm the calculation for the distance of IGR J16479-4514 using the distance modulus. The distances of IGR J16479-4514 assuming the aforementioned spectral types are reported in Table 12 using the values for $M_{\rm V}$ obtained from Wegner (2006) and Martins & Plez (2006). We find that the distance of stars with spectral type O7 I and earlier to be between 4.4–4.6 kpc, which are resonably consistent with the measurements in Rahoui et al. (2008).

IGR J16479-4514 is a heavily absorbed SFXT where the $N_{\rm H}$ was measured to be $9.5\pm0.3\times10^{22}$ atoms

[3] http://www.iasfbo.inaf.it/~masetti/IGR/sources/16418.html

TABLE 12
POSSIBLE PARAMETERS OF CANDIDATE DONOR STARS FOR IGR J16479-4514

Spectral Type	$M/M_\odot$	q	$R/R_\odot$	$R_L/R_\odot$ [a]	R_L/R	M_V	$(J-K)_0$ [a]	$E(J-K)$ [a]	i° [b]	d_{sun} [c] (kpc)	d_{sun} [d] (kpc)
O6 Ia	44.10	0.032	19.95	22.03	0.91	*-6.38*	-0.21	3.48	69–75	4.44	4.50
O6.5 Ia	41.20	0.034	20.22	21.42	0.94	*-6.38*	-0.21	3.48	66–71	4.46	4.56
O7 Ia	38.44	0.036	20.49	20.80	0.99	*-6.38*	-0.21	3.48	63–68	4.46	4.62
O7.5 Ia	36.00	0.039	20.79	20.23	1.03	*-6.38*	-0.21	3.48	60–64	4.48	4.69
O8 Ia	33.72	0.042	21.10	19.68	1.07	*-6.36*	-0.21	3.48	58–61	4.44	4.81

NOTE.—Possible Parameters of Candidate Donor Stars.
[a] The value for $(J-K)_0$ was calculated using $(J-H)_0$ and $(H-K)_0$ published in Martins & Plez (2006). $E(J-K)$ is found by subtracting $(J-K)_0$ from the observed $J-K$
[b] The range of inclination angles of the system consistent with the measured eclipse half-angle.
[c] The distance the object is from the Sun using the distance modulus.
[d] The distance the object is from the Sun using the radius to distance ratio derived from spectral energy distribution. The radius to distance ratio is found to be 1×10^{-10} (Chaty et al. 2008).

cm^{-2} (Sidoli et al. 2013). This is an order of magnitude larger than the Galactic H I values reported by the Leiden/Argentine/Bonn survey (Kalberla et al. 2005) and in the review by Dickey & Lockman (1990), which are 1.87×10^{22} and 2.14×10^{22} atoms cm^{-2}, respectively. Since the measured N_H for both sources was found to be in excess of the Galactic H I, determining the interstellar fraction of N_H is difficult. Therefore, we cannot verify the value for the extinction in Rahoui et al. (2008) without the presence of systematic error.

We calculate the reddening values $E(J-K)$ for each proposed spectral type for the mass donor (see Table 12) using the observed value of the $J-K$ color of 3.27[4] and the intrinsic $(J-K)_0$ for the proposed mass donors (see Table 12). To check for consistency with late O supergiant stars, we compare this with the reddening in the $B-V$ band using Equation 1 in Güver & Oumlzel (2009) and the extinction in the V-band (A_V) (Rahoui et al. 2008). Converting $E(B-V)$ to $E(J-K)$ using Table 3 in Rieke & Lebofsky (1985), we find the reddening in the $E(J-K)$ band to be 3.12. While this is slightly lower than what would be expected for late O supergiant spectral types, the presence of systematic errors, described above prevents an exact calculation.

Stars with spectral type O7 I and earlier satisfy the eclipse duration and Roche-lobe constraints (see Figure 20). Determining the interstellar fraction of N_H is difficult since the measured N_H is greatly in excess of interstellar values. We find the distance of the proposed counterparts to be consistent with those determined by Rahoui et al. (2008). Since no pulsation period was identified, the next step to constrain the donor star would be radial velocity measurements in the near-infrared.

4.1.4. IGR J18027-2016

Our results show that the mass and radius of the donor star in IGR J18027-2016 can be constrained to be between $18.6\pm0.9\,M_\odot$ and $17.4\pm0.9\,R_\odot$ and $19.4\pm0.9\,M_\odot$ and $19.5^{+0.8}_{-0.7}\,R_\odot$ for edge-on orbits and inclinations where the Roche-lobe is completely filled, respectively. We find the inclination where the Roche-lobe is filled to be 73.3°, which is consistent with the earlier results from Mason et al. (2011). Since the semi-amplitude of the radial velocities of both the donor star and compact object are known, we also find that the mass of the neutron star can be constrained. We calculate the mass of the

[4] http://www.iasfbo.inaf.it/~masetti/IGR/sources/16479.html

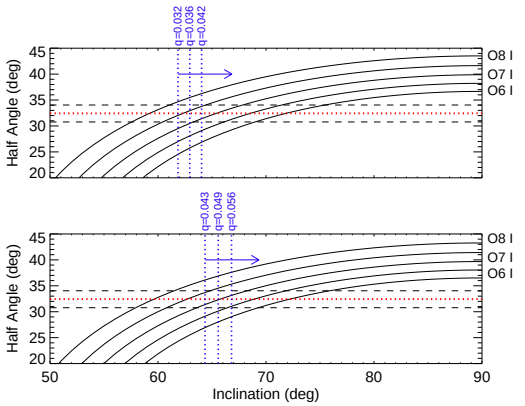

Fig. 20.— The black curves show the predicted eclipse half angle as a function of inclination angle for stars with the candidate spectral types for IGR J16479-4514. The red and black dashed lines indicate the eclipse half angle and estimated error as measured by *Swift* BAT. We assume a neutron star mass of 1.4 $M_\odot$ (top) and of mass 1.9 $M_\odot$ (bottom) and typical masses and radii for the assumed companion spectral type (see Table 12). The blue vertical dashed lines indicate the lower limit of the inclination angle. Inclinations to the left of these correspond to stars that overfill the Roche-lobe.

neutron star to be between 1.37±0.19 $M_\odot$ and 1.43±0.20 $M_\odot$ for our lower and upper limits (see Section 3.4).

Since the radius of the donor star is constrained, we also can estimate the distance, optical and near infrared magnitudes of IGR J18027-2016. Using SED measurements, Chaty et al. (2008) calculated the radius to distance ratio to be $4\pm1\times10^{-11}$, where the uncertainties are at the 90% confidence interval. At the 90% confidence interval, we find the eclipse half-angle to be $34^{+4\circ}_{-3}$ and the radius of the donor star to be constrained to between 17^{+2}_{-1} $R_\odot$ and 19±1 $R_\odot$ in the two limits described in Section 3.4. Combining our results for the radius of the donor star with the radius to distance ratio (Table 6; Chaty et al. 2008), we find that the distance of IGR J18027-2016 can be constrained to 11±2 kpc and 12±2 kpc in the two limits. Using the distance modulus (e.g. Nespoli et al. 2008), the absolute magnitude of IGR J18027-2016 can be calculated. The apparent magnitude in the R-band, R, and the extinction in the V-band, A_V were found to be 16.9 and 8.5 (Masetti et al. 2008). We find the absolute magnitude in the R-band, M_R to be ∼-5 at both constraints, which is what would be expected for a B-type supergiant (Martins & Plez 2006; Wegner 2006).

Our results are consistent with the previously proposed B1 Ib (Torrejón et al. 2010) or B0-B1 I (Mason et al. 2011) spectral types in IGR J18027-2016. We constrain the mass and radius of the donor star to be between 18.6–19.4 $M_\odot$ and 17.4–19.5 $R_\odot$. We also constrain the mass of the neutron star to be 1.18–1.63 $M_\odot$, which marginally improves on the results in Mason et al. (2011), which was found to be 1.15–1.85 $M_\odot$.

4.1.5. XTE J1855-026

We find that the mass and radius of the donor star in XTE J1855-026 are constrained between 19.6±1.1 $M_\odot$ and 21.5±0.5 $R_\odot$ at edge-on orbits to 20.2±1.2 $M_\odot$ and 23.0±0.5 $R_\odot$ where the Roche-lobe is just filled. The inclination where the Roche-lobe is filled is found to be 76.4°. We find the derived masses and radii to be consistent with those reported in Carroll & Ostlie (2006) and Allen (2000) for stars with spectral type B0 I. Since the semi-amplitude of the radial velocities for both the donor star and compact object are known, we find that the mass of the neutron star can be constrained to be between 1.77±0.55 $M_\odot$ and 1.82±0.57 $M_\odot$ (see Section 3.5). We note that the large error estimates in the mass of the neutron star are likely to be attributed to substantial uncertainties in the estimate in K_o as reported in González-Galán (2015). This is likely to be attributed to emission line contamination and/or changes in the stellar wind.

Based on optical and near-infrared spectra together with the analysis reported in Verrecchia et al. (2002), the spectral type of the donor star was previously determined to be a B0 Iaep (Negueruela et al. 2008). Based on the ratio of the equivalent widths of Si IV to Si III which is a diagnostic for supergiant spectral types (Walborn 1971), the mass donor was recently refined to a BN0.2 Ia by González-Galán (2015). Using SED measurements, Coleiro & Chaty (2013) calculated the radius and distance to be 26.9 $R_\odot$ and 10.8±1.0 kpc, which places XTE J1855-026 in the Scutum arm region. Combining the properties of the newly derived spectral type with the dis-

tance modulus, González-Galán (2015) recently calculated the nominal distance of XTE J1855-026 to be 10^{+7}_{-4} kpc. Based on these results, the radius to distance ratio can be calculated to be $5.6\pm0.5\times10^{-11}$. Combining our results for the radius of the donor star with the calculated radius to distance ratio, we find the distance of XTE J1855-026 can be constrained to 8.6 ± 0.8 kpc and 9.2 ± 0.9 kpc in the two limits.

Corbet et al. (1999) measured the $N_{\rm H}$ in XTE J1855-026 to be $14.7\pm0.6\times10^{22}$ atoms cm^{-2}, which exceeds the values reported by the Leiden/Argentine/Bonn survey (Kalberla et al. 2005) and in the review by Dickey & Lockman (1990). In a *Swift* XRT observation, the $N_{\rm H}$ was found to be $4.1\pm0.5\times10^{22}$ atoms cm^{-2} (Romano et al. 2008). These are signifcantly larger than the measurements for the interstellar $N_{\rm H}$, which are 6.62×10^{21} atoms cm^{-2} (Kalberla et al. 2005) and 7.35×10^{21} atoms cm^{-2} (Dickey & Lockman 1990). Since the measured $N_{\rm H}$ was found to be in excess of the Galactic H I, the conversion between the interstellar $N_{\rm H}$ and the extinction $A_{\rm V}$ is problematic and the value of 5.8 ± 0.9 in Coleiro & Chaty (2013) cannot be verified without the presence of systematic error.

4.2. What is the nature of the non-zero eclipse flux in IGR J16393-4643?

The source flux during eclipse in IGR J16393-4643 does not reach 0 counts s^{-1} in the folded light curves (see Figure 4). We find the ratio between the flux during eclipse to the flux outside eclipse to be $54\pm5\%$. This is significantly larger than what is observed in the other XRBs in our study (see Table 1).

We first discuss the possible scenario where we observe a partial eclipse in IGR J16393-4643. In our model for the eclipse (see Section 2.2), we assume the compact object to be a point source (Joss & Rappaport 1984). While this is a valid assumption since the radius of the compact object is much smaller than that of the donor star, our approximation does not consider the extended X-ray emission region. In this case, the constraints the mass and radius of the donor star must take into account the size of the extended emission region. Since a significant residual flux is observed, it is likely that we observe a partial eclipse.

We also consider the possibility that the residual emission observed in IGR J16393-4643 is attributed to a dust-scattering halo similar to what is observed in some other HMXBs (Cen X-3; Vela X-1; OAO 1657-415, Day & Tennant 1991; Woo et al. 1994; Audley et al. 2006). While residual emisison has been attributed to a dust-scattering in some other HMXBs, the residual emission found in IGR J16393-4643 in the BAT folded light curves (15–50 keV) is seen at much higher levels (see Table 1). A dust-scattering halo is predominantly a soft X-ray phenomenon. While a significant fraction of the out-of-eclipse flux may be in a dust-scattering halo (Predehl & Schmitt 1995), we expect a smaller fraction to be in the energies resolved by BAT (e.g. Coley et al. 2014, and references therein). Therefore, we conclude a dust-scattering halo cannot be the sole mechanism responsible for the residual emission seen in the folded light curves.

Finally, we discuss the possibility that Compton scattering and reprocessing in a region of dense gas could account for the residual flux in eclipse. Bodaghee et al. (2006) found that a Compton emission (`comptt` within Xspec) model with an electron temperature of 4.4 ± 0.3 keV and optical depth of 9 ± 1 provides a good fit to the average spectrum of IGR J16393-4643. Additionally, Fe Kα and Fe Kβ lines were found at 6.4 keV and 7.1 keV, respectively, where the ratio of the iron intensities is seen to be consistent with photoionization (Bodaghee et al. 2006; Kaastra & Mewe 1993; Islam et al. 2015). The equivalent widths (EQW) in the *XMM-Newton* observation were found to be 60 ± 30 eV and an upper limit of 120 eV, for the Fe Kα and Fe Kβ lines respectively (Bodaghee et al. 2006). In a recent *Suzaku* observation, the EQW of the Fe Kα and Fe Kβ lines were found to be 46^{+7}_{-6} eV and an upper limit of 30 eV (Islam et al. 2015). While the mechanism responsible for the Fe Kα and Fe Kβ is likely to be fluorescence of cold matter, the equivalent widths point to a likely origin in a spherical distribution of dense gas (Bodaghee et al. 2006). Therefore, Compton scattering and reprocessing might be the sole contributor to the residual emission observed in the BAT folded light curves.

It is likely that a combination of the mechanisms described above account for the residual emission found in the folded light curves of IGR

J16393-4643 (see Section 3.1). Since the count rate during eclipse is significantly larger than what is observed in most other eclipsing HMXBs, it is likely that only a small fraction comes from a dust-scattering halo.

4.3. What mechanism is responsible for asymmetries in the eclipse profile?

The eclipse profiles show the presence of asymmetries (see Tables 2 and 3) as previously noted by Falanga et al. (2015) in the cases of IGR J18027-2016 and XTE J1855-026 and Jain et al. (2009) in the case of IGR J16479-4514. These asymmetries seen in the ingress and egress durations are suggestive of the presence of complex structures in the wind such as accretion or photoionization wakes.

We first discuss the possible case that the asymmetry in the eclipse profiles can be attributed to accretion wakes. In an HMXB driven entirely by a spherical wind, material is only accreted in a cylindrical region where the kinetic energy is less than the gravitational potential energy of the compact object. The radius of the accretion cylinder is the Bondi-Hoyle accretion radius (Equation 1, Feldmeier et al. 1996). Perturbed material forms an "accretion wake" that typically trails the orbit of the neutron star and results in large intrinsic column densities (Blondin et al. 1990). Prior to eclipse, the progressively increasing $N_{\rm H}$ partially obscures the X-ray emission resulting in longer ingress durations compared to the duration of egress. Since the accretion wake is located beyond the compact object during egress, no apparent increase in the intrinsic $N_{\rm H}$ is observed. The ingresses observed are somewhat larger than egress, which is consistent with the presence of an accretion wake (Blondin et al. 1990). The count rate prior to ingress is also somewhat smaller than that observed after egress, providing additional evidence for accretion wakes. Hardness ratios or measurements of $N_{\rm H}$ folded on the orbital period could be implemented to confirm the possibility of accretion wakes.

We also consider the possibility that photoionization wakes could explain the asymmetric eclipse profiles. The eclipse profiles of IGR J18027-2016 and XTE J1855-026 are compared to those seen in eclipsing systems where asymmetric density enhancements are observed on large spatial dimensions (e.g. Vela X-1; Feldmeier et al. 1996). In systems where the X-ray luminosity is significantly high, a switch-off of the radiative driving force could lead to a reduced wind velocity and enhanced wind density (Feldmeier et al. 1996). This enhanced X-ray scattering region trails the neutron star and results in ingress durations that are significantly larger than those observed at egress (Feldmeier et al. 1996). The eclipse profiles of IGR J18027-2016 and XTE J1855-026 differ from those expected from a photoionization wake– the ingress duration in Vela X-1 was seen to be ϕ =0.11 (Feldmeier et al. 1996).

We additionally discuss how energy dependence in the asymmetric eclipse profiles can arise. The high $N_{\rm H}$, on the order of 10^{23} atoms cm^{-2}, implies the presence of a strong circumstellar wind (Kuulkers 2005), and the X-ray absorption due to this will lead to sharper ingress and egress transitions compared to that seen at lower energies. In a *Suzaku* observation of IGR J16479-4514 that covers part of the eclipse, Sidoli et al. (2013) found the egress transition to be broader in soft energies. In their review, Falanga et al. (2015) found asymmetries to be slightly enhanced at lower energies compared to higher energies. While investigating the energy dependence in the eclipse transitions is beyond the scope of the present paper, this study in obscured SGXBs will be difficult due to a reduced count rate at low energies that results from the large intrinsic absorption present in these systems (Falanga et al. 2015).

Finally, we consider the possibility that the asymmetric eclipse profiles could be attributed to a small to modest eccentricity. Since we considered objects with relatively short orbital periods, we expect the eccentricity of the systems to be near zero (Zahn 1977; Maccarone et al. 2014). The eccentricity in IGR J18027-2016 and XTE J1855-026 were both noted to be small to modest, where e was found to be less than 0.2 and 0.04, respectively (Augello et al. 2003; Corbet & Mukai 2002). In the cases of IGR J16393-4643, IGR J16418-4532 and IGR J16479-4514 where no pulse-timing or radial-velocity methods are available to determine an orbital solution, we constrain the maximum allowed eccentricity to that where the radius of the donor star completely fills the Roche-lobe at periastron (Goossens et al. 2013, and references therein). These were all found to

be near zero (see Figure 21). Since the eccentricities are found to be small to modest, we do not expect these to result in sizeable asymmetries in the eclipse profile. Additionally, apsidal advance will be apparent in the case that an eccentric orbit could lead to asymmetries in the eclipse profile. While apsidal advance would be difficult to detect in the $\sim$9 yr of *Swift* data, we believe it to be unlikely for asymmetries to be solely attributed to small to modest eccentricities. Furthermore, accurate measurements of apsidal advance will depend on multiple pulse-timing measurements of these systems, which are not yet available.

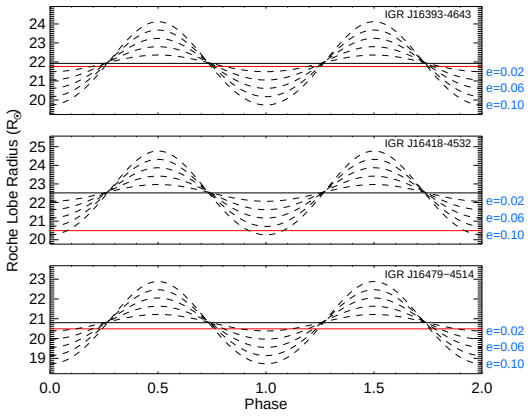

Fig. 21.— A sample plot of the Roche-lobe of the donor stars in IGR J16393-4643 (top), IGR J16418-4532 (middle) and IGR J16479-4514 (bottom) vs. orbital phase for eccentricities ranging from 0.0 to 0.1 in steps of 0.02. The horizontal red line represents the radius of the donor star under the assumption that the donor is an O9 I for IGR J16393-4643 and O7 I for both IGR J16418-4532 and IGR J16479-4532 (Martins et al. 2005).

5. Conclusion

Eclipsing X-ray binaries provide an opportunity to constrain the physical parameters of the donor star as well as the compact object. To determine the eclipse half-angle in our survey, we modeled the eclipses using both symmetric and asymmetric step-and-ramp functions. The luminosity of each system is less than expected for Roche-lobe overflow (Kaper et al. 2004), which means we can attach the constraint that the mass donor underfills the Roche-lobe. Since IGR J18027-2016 and XTE J1855-026 are the only "double-lined binaries" in our sample, we calculate the parameters of the other systems assuming the neutron stars to be at the white-dwarf Chandrasekhar limit, $1.4 M_{\odot}$. We also calculated the parameters of the other systems assuming a more massive neutron star– $1.9 M_{\odot}$.

Our results show that stars with spectral type B III satisfy both constraints imposed by the eclipse duration and Roche-lobe for IGR J16393-4643. Assuming the estimates for the mass and radius of a B5 III star reported in Carroll & Ostlie (2006), we find the mass and radius of the donor star to exceed $7\,M_{\odot}$ and $6.3\,R_{\odot}$. B I stars were found to overfill the Roche-lobe. The source emission in IGR J16393-4643 does not reach 0 counts s^{-1} in the folded light curves, where the fraction between the flux in eclipse to that outside eclipse was found to be 54±5% (see Tables 1– 3). Compton scattering and reprocessing in a dense region of gas could possibly account for the X-ray emission region not obscured by the donor star.

Our results show that the previously proposed O8.5 I and BN0.5 Ia spectral types for the mass donor in IGR J16418-4532 must be excluded. While these spectral types satisfy the eclipse half-angle, the Roche-lobe is significantly overfilled. Stars with spectral type O7.5 I or earlier are consistent with both the eclipse half-angle and the Roche-lobe. In this case, we find the mass and radius of the donor star to exceed $36.00\,M_{\odot}$ and $20.79\,R_{\odot}$ assuming the estimates for the mass and radius of an O7.5 I star reported in Martins et al. (2005). We find the minimum inclination angle of the system to be 67°. The distance measurements of IGR J16418-4532 are consistent with the previously determined distance (see Table 11); however, determining the interstellar fraction of $N_{\rm H}$ was found to be problematic. The ingress and egress durations in the folded light curves were found to be asymmetric where the ingress duration is longer than the egress duration. This is likely attributed to the presence of an accretion wake or from a focused stream as noted in Sidoli et al. (2012) and Drave et al. (2013).

The previously proposed O8.5 Ia and O9.5 Iab spectral classifications of the mass donor in IGR J16479-4514 must be excluded because the Roche-lobe is significantly overfilled. However, we found that stars with spectral type O7 I and earlier sat-

isfy both constraints imposed by the eclipse duration and Roche-lobe. Assuming the estimates for the mass and radius of an O7 I star reported in Martins et al. (2005), the mass and radius of the donor star are found to exceed $38.44\,M_\odot$ and $20.49\,R_\odot$, respectively. We find the minimum inclination angle of the system to be 63°. The distance measurements remain unchanged from earlier measurements (see Table 12); however, the interstellar fraction of $N_{\rm H}$ remains undetermined. We find the ingress and egress durations to be symmetric within the error bars. The ratio between the radius of the donor star and Roche-lobe was found to exceed 0.9, which shows the possibility of transitional Roche-lobe overflow.

The mass and radius of the donor star in IGR J18027-2016 was constrained to $18.6\pm0.9\,M_\odot$ and $17.4\pm0.9\,R_\odot$ and $19.4\pm0.9\,M_\odot$ and $19.5^{+0.8}_{-0.7}\,R_\odot$ in the two limits. We find the inclination angle where the donor star just fills the Roche-lobe size to be 73.3°. We also find the distance measurements of IGR J18027-2016 to be 11 ± 2 kpc and 12 ± 2 kpc in the allowed limits. In the allowed limits, we constrained mass of the neutron star to between $1.37\pm0.19\,M_\odot$ and $1.43\pm0.20\,M_\odot$. The folded light curve shows complicated and asymmetric ingress and egress durations, which can be explained either by the presence of accretion wakes.

Our results show the mass and radius of the donor star in XTE J1855-026 to be constrained to $19.6\pm1.1\,M_\odot$ and $21.5\pm0.5\,R_\odot$ at edge-on orbits to $20.2\pm1.2\,M_\odot$ and $23.0\pm0.5\,R_\odot$ where the Roche-lobe size is just filled. We find the inclination angle where the donor star just fills the Roche-lobe size to be 76.4 degrees. In the allowed limits, we find the distance of XTE J1855-026 can be constrained to 8.6 ± 0.8 kpc and 9.2 ± 0.9 kpc. We find the mass of the neutron to be constrained between $1.77\pm0.55\,M_\odot$ and $1.82\pm0.57\,M_\odot$. Complicated and asymmetric ingress and egress durations were seen in the folded light curve, which suggests the presence of complex structure in the wind.

To further constrain the physical parameters of the donor star and the compact object in all these systems, additional observations are required. Constraining the mass of the neutron star will help constrain the Equation-of-State. Since the pulse period has been accurately measured, for IGR J16393-4643 and IGR J16418-4532 the study would benefit from both pulse-timing analysis as well as radial-velocity curves in the near-infrared. A radial-velocity curve in the optical or near-infrared would provide additional constraints for IGR J16479-4514 where a pulse-period has yet to be identified.

We thank the anonymous referee for useful comments and support from NASA 14-ADAP14-0167.

REFERENCES

Allen, K. W. 2000, Astrophysical quantities., by Allen, K. W.. Translated from the 4. revised and suppl. English edition. Moskva: Mir, 448 p.,

Ash, T. D. C., Reynolds, A. P., Roche, P., et al. 1999, MNRAS, 307, 357

Audley, M. D., Nagase, F., Mitsuda, K., Angelini, L., & Kelley, R. L. 2006, MNRAS, 367, 1147

Augello, G., Iaria, R., Robba, N. R., et al. 2003, ApJ, 596, L63

Barthelmy, S. D., Barbier, L. M., Cummings, J. R., et al. 2005, Space Sci. Rev., 120, 143

Blondin, J. M., Kallman, T. R., Fryxell, B. A., & Taam, R. E. 1990, ApJ, 356, 591

Blondin, J. M., & Owen, M. P. 1997, IAU Colloq. 163: Accretion Phenomena and Related Outflows, 121, 361

Bodaghee, A., Walter, R., Zurita Heras, J. A., et al. 2006, A&A, 447, 1027

Bodaghee, A., Rahoui, F., Tomsick, J. A., & Rodriguez, J. 2012, ApJ, 751, 113

Bowers, R. L., & Deeming, T. 1984, Astrophysics. Vol. I: Stars. Vol. II: Interstellar matter and galaxies.. R. L. Bowers, T. Deeming.Jones and Bartlett Publishers, Inc., 20 Park Plaza, Boston, Mass. 02116, USA. Vol. I: 344 pp., Vol. II: 244 pp. ISBN 0-86720-018-9(Vol. I), ISBN 0-86720-047-2 (Vol. II).

Bozzo, E., Stella, L., Israel, G., Falanga, M., & Campana, S. 2009, American Institute of Physics Conference Series, 1126, 319

Carroll, B. W., & Ostlie, D. A. 2006; Institute for Mathematics and Its Applications; Weber State University, Inc.; Addison-Wesley Publishing Company; Reading, Massachusetts

Chakrabarty, D., Grunsfeld, J. M., Prince, T. A., et al. 1993, ApJ, 403, L33

Chakrabarty, D. 1996, Ph.D. Thesis, California Institute of Technology

Chandrasekhar, S. 1931, ApJ, 74, 81

Chaty, S., Rahoui, F., Foellmi, C., et al. 2008, A&A, 484, 783

Coleiro, A., & Chaty, S. 2013, ApJ, 764, 185

Coleiro, A., Chaty, S., Zurita Heras, J. A., Rahoui, F., & Tomsick, J. A. 2013, A&A, 560, A108

Coley, J. B., Corbet, R. H. D., Mukai, K., & Pottschmidt, K. 2014, ApJ, 793, 77

Corbet, R. H. D. 1986, MNRAS, 220, 1047

Corbet, R. H. D., Marshall, F. E., Peele, A. G., & Takeshima, T. 1999, ApJ, 517, 956

Corbet, R. H. D., & Mukai, K. 2002, ApJ, 577, 923

Corbet, R. H. D., Markwardt, C. B., & Swank, J. H. 2005, ApJ, 633, 377

Corbet, R., Barbier, L., Barthelmy, S., et al. 2006, The Astronomer's Telegram, 779, 1

Corbet, R., Markwardt, C., Barbier, L., et al. 2007, Progress of Theoretical Physics Supplement, 169, 200

Corbet, R. H. D., Krimm, H. A., Barthelmy, S. D., et al. 2010, The Astronomer's Telegram, 2570, 1

Corbet, R. H. D., & Krimm, H. A. 2013, ApJ, 778, 45

Cusumano, G., La Parola, V., Segreto, A., et al. 2010, A&A, 510, A48

Day, C. S. R., & Tennant, A. F. 1991, MNRAS, 251, 76

Dickey, J. M., & Lockman, F. J. 1990, ARA&A, 28, 215

Drave, S. P., Bird, A. J., Sidoli, L., et al. 2013, MNRAS, 433, 528

Drave, S. P., Bird, A. J., Goossens, M. E., et al. 2013, The Astronomer's Telegram, 5131, 1

Eggleton, P. P. 1983, ApJ, 268, 368

Falanga, M., Bozzo, E., Lutovinov, A., et al. 2015, A&A, 577, A130

Feldmeier, A., Anzer, U., Boerner, G., & Nagase, F. 1996, A&A, 311, 793

González-Galán, A. 2015, arXiv:1503.01087

Goossens, M. E., Bird, A. J., Drave, S. P., et al. 2013, MNRAS, 434, 2182

Gray, R. O., & Corbally, C., J. 2009, Stellar Spectral Classification by Richard O. Gray and Christopher J. Corbally. Princeton University Press, 2009. ISBN: 978-0-691-12511-4,

Güver, T., Oumlzel, F. 2009, MNRAS, 400, 2050

Hill, A. B., Walter, R., Knigge, C., et al. 2005, A&A, 439, 255

Horne, J. H., & Baliunas, S. L. 1986, ApJ, 302, 757

Islam, N., Maitra, C., Pradhan, P., & Paul, B. 2015, MNRAS, 446, 4148

Islam, N., & Paul, B. 2014, MNRAS, 441, 2539

Jain, C., Paul, B., & Dutta, A. 2009, MNRAS, 397, L11

Jain, C., Paul, B., & Dutta, A. 2009, Research in Astronomy and Astrophysics, 9, 1303

Joss, P. C., & Rappaport, S. A. 1984, ARA&A, 22, 537

Kaastra, J. S., & Mewe, R. 1993, A&AS, 97, 443

Kalberla, P. M. W., Burton, W. B., Hartmann, D., et al. 2005, A&A, 440, 775

Kaper, L., van der Meer, A., & Tijani, A. H. 2004, Revista Mexicana de Astronomia y Astrofisica Conference Series, 21, 128

Kaper, L., van der Meer, A., van Kerkwijk, M., & van den Heuvel, E. 2006, The Messenger, 126, 27

Krimm, H. A., Holland, S. T., Corbet, R. H. D., et al. 2013, ApJS, 209, 14

Kuulkers, E. 2005, Interacting Binaries: Accretion, Evolution, and Outcomes, 797, 402

Lattimer, J. M. 2012, Annual Review of Nuclear and Particle Science, 62, 485

Lefever, K., Puls, J., & Aerts, C. 2007, A&A, 463, 1093

Levine, A. M., Bradt, H. V., Chakrabarty, D., Corbet, R. H. D., & Harris, R. J. 2011, ApJS, 196, 6

Maccarone, T. J., Girard, T. M., & Casetti-Dinescu, D. I. 2014, MNRAS, 440, 1626

Manousakis, A., & Walter, R. 2011, A&A, 526, AA62

Martins, F., Schaerer, D., & Hillier, D. J. 2005, A&A, 436, 1049

Martins, F., & Plez, B. 2006, A&A, 457, 637

Masetti, N., Mason, E., Morelli, L., et al. 2008, A&A, 482, 113

Mason, A. B., Norton, A. J., Clark, J. S., Negueruela, I., & Roche, P. 2010, A&A, 509, A79

Mason, A. B., Norton, A. J., Clark, J. S., Negueruela, I., & Roche, P. 2011, A&A, 532, A124

Mason, A. B., Clark, J. S., Norton, A. J., et al. 2012, MNRAS, 422, 199

Massa, D., Prinja, R. K., & Fullerton, A. W. 1995, ApJ, 452, 842

Molkov, S., Mowlavi, N., Goldwurm, A., et al. 2003, The Astronomer's Telegram, 176, 1

Negueruela, I., Casares, J., Verrecchia, F., et al. 2008, The Astronomer's Telegram, 1876, 1

Nespoli, E., Fabregat, J., & Mennickent, R. E. 2008, The Astronomer's Telegram, 1450, 1

Nespoli, E., Fabregat, J., & Mennickent, R. E. 2008, A&A, 486, 911

Pearlman, A. B., Corbet, R., & Pottschmidt, K. 2013, American Astronomical Society Meeting Abstracts #221, 221, #142.38

Predehl, P., & Schmitt, J. H. M. M. 1995, A&A, 293, 889

Rahoui, F., Chaty, S., Lagage, P.-O., & Pantin, E. 2008, A&A, 484, 801

Raichur, H., & Paul, B. 2010, MNRAS, 401, 1532

Rappaport, S. A., & Joss, P. C. 1983, Accretion-Driven Stellar X-ray Sources, 13

Ray, P. S., & Chakrabarty, D. 2002, ApJ, 581, 1293

Rieke, G. H., & Lebofsky, M. J. 1985, ApJ, 288, 618

Romano, P., Mereghetti, S., Sidoli, L., & Evans, P. A. 2008, The Astronomer's Telegram, 1875, 1

Romano, P., Sidoli, L., Cusumano, G., et al. 2009, MNRAS, 399, 2021

Romano, P., Mangano, V., Ducci, L., et al. 2012, MNRAS, 419, 2695

Rubin, B. C., Finger, M. H., Harmon, B. A., et al. 1996, ApJ, 459, 259

Scargle, J. D. 1982, ApJ, 263, 835

Scargle, J. D. 1989, ApJ, 343, 874

Searle, S. C., Prinja, R. K., Massa, D., & Ryans, R. 2008, A&A, 481, 777

Seward, F. D., & Charles, P. A. 1995, Exploring the X-Ray Universe, by Frederick D. Seward and Philip A. Charles, pp. 414. ISBN 0521437121. Cambridge, UK: Cambridge University Press, November 1995.,

Sidoli, L., Esposito, P., Sguera, V., et al. 2013, MNRAS, 429, 2763

Sidoli, L., Mereghetti, S., Sguera, V., & Pizzolato, F. 2012, MNRAS, 420, 554

Sugizaki, M., Mitsuda, K., Kaneda, H., et al. 2001, ApJS, 134, 77

Thompson, T. W. J., Tomsick, J. A., Rothschild, R. E., in't Zand, J. J. M., & Walter, R. 2006, ApJ, 649, 373

Thompson, T. W. J., Tomsick, J. A., in 't Zand, J. J. M., Rothschild, R. E., & Walter, R. 2007, ApJ, 661, 447

Tomsick, J. A., Lingenfelter, R., Corbel, S., Goldwurm, A., & Kaaret, P. 2004, The Astronomer's Telegram, 224, 1

Torrejón, J. M., Negueruela, I., Smith, D. M., & Harrison, T. E. 2010, A&A, 510, A61

Tueller, J., Baumgartner, W. H., Markwardt, C. B., et al. 2010, ApJS, 186, 378

Val Baker, A. K. F., Norton, A. J., & Quaintrell, H. 2005, A&A, 441, 685

Verrecchia, F., Negueruela, I., Covino, S., & Israel, G. 2002, The Astronomer's Telegram, 102, 1

Walborn, N. R. 1971, ApJS, 23, 257

Walter, R., Zurita Heras, J., Bassani, L., et al. 2006, A&A, 453, 133

Wegner, W. 2006, MNRAS, 371, 185

Woo, J. W., Clark, G. W., Day, C. S. R., Nagase, F., & Takeshima, T. 1994, ApJ, 436, L5

Zahn, J.-P. 1977, A&A, 57, 383

This 2-column preprint was prepared with the AAS LaTeX macros v5.2.